Central Schemes on Overlapping Cells

Dedicated to James Glimm on the occasion of his 70th birthday

Yingjie Liu*

Abstract

Nessyahu and Tadmor's central scheme (J. Comput. Phys, 87(1990)) has the benefit of not using Riemann solvers or characteristic decomposition for solving hyperbolic conservation laws and related convection diffusion equations. But the staggered averaging causes large dissipation when the time step size is small comparing to the mesh size. The recent work of Kurganov and Tadmor (J. Comput. Phys, 160(2000)) overcomes the problem by use of a variable control volume and obtains a semi-discrete non-staggered central scheme. Motivated by this work, we introduce overlapping cell averages of the solution at the same discrete time level, and develop a simple alternative technique to control the $O(1/\Delta t)$ dependence of the dissipation. Semi-discrete form of the central scheme can also be obtained to which the TVD Runge-Kutta time discretization of Shu and Osher (J. Comput. Phys, 77(1988)) can be applied. This technique is essentially independent of the reconstruction and the shape of the mesh, thus could also be useful for unstructured mesh. The overlapping cell representation of the solution also opens new possibilities for reconstructions. Generally more compact reconstruction can be achieved. We demonstrate through numerical examples that combining two classes of the overlapping cells in the reconstruction can achieve higher resolution.

Keywords. Central Scheme, ENO scheme, MUSCL scheme, TVD scheme.
AMS subject classification. 65M60, 65M12

*School of Mathematics, Georgia Institute of Technology, Atlanta, GA 30332 (yingjie@math.gatech.edu).

1 Introduction

The central Nessyahu and Tadmor (NT) scheme provides a black box solution to nonlinear hyperbolic conservation laws and other closely related equations by use of the staggered average to avoid dealing with the solutions within the Riemann fans. When supplied with high order accurate non-oscillatory reconstruction techniques (e.g., MUSCL [32], ENO [10] etc), various variations of the central schemes can be developed to solve different problems.

In Liu and Tadmor [25], a third order non-oscillatory central scheme is developed. In Levy, Puppo and Russo [20, 21, 22], a series of central WENO schemes have been developed with increased order of accuracy. In Jiang *et. al.* [11], a general procedure is introduced to develop central schemes on non-staggered grid. Convex higher order ENO scheme without characteristic decomposition or staggered grids has been developed in Liu and Osher [23]. Since the central schemes usually use staggered average, the time step size cannot be passed to zero. One can easily see this by assuming the flux of the hyperbolic conservation laws is zero, then what the central scheme does is conservative rezoning at every time step, which will gradually smear out the solution as the number of iteration increases. Similar situation occurs in the 2D conservative front tracking and is overcome by use of space-time cells in Glimm *et. al.* [8]. Central schemes typically require the approximation of the flux integrated over time which in turn requires the evaluation of the flux at middle time steps. In Bianco, Puppo and Russo [5], the natural continuous extension of Runge-Kutta method (Zennaro [34]) is used in the evaluation of the flux integral which greatly improves the efficiency for higher order central schemes. In Arminjon and St-Cyr [1], solutions in previous time levels are used in the prediction of the flux at middle time steps which reduces the computational cost in multi space dimension.

In [15], Kurganov and Tadmor introduce a new kind of central scheme without the large dissipation error related to the small time step size by use of a variable control volume whose size depends on time step size. By passing the limit as time step size goes to zero, the semi-discrete central scheme scheme can be developed. This allows the central scheme to be used for a larger class of equations where time step size has to be small comparing to the mesh size. This also results in a non-staggered central scheme and allows the use of TVD Runge-Kutta time discretization methods of Shu and Osher [29]. Higher order semi-discrete central schemes are developed, e.g. in

Kurganov and Petrova [17], Kurganov and Levy[14].

In this paper, we introduce an alternative technique to control the dissipative error of central schemes. The major idea is to introduce overlapping cell representation of the solution. An immediate advantage is that the time discretization becomes simple by use of the TVD Runge-Kutta method. Also by use of a time step size dependent convex combination of the overlapping cell averages, the $O(1/\Delta t)$ dependent dissipative error can be easily controlled. The computational cost related to the use of overlapping cell averages should be compensated by these benefits and by more efficient reconstruction methods using the combined information from the overlapping cell averages. Bryson and Levy [6] develop high order central WENO schemes for multi-dimensional Hamilton-Jacobi equations which use a diagonal reconstruction strategy to project the solution at old evolution points to the regular grid points. A similar strategy is also used in our 2D diagonal line method in order to take full advantage of the information from the combined overlapping cells.

In section 2 we will introduce the 1D formulation of the central scheme on overlapping cells and introduce the technique to control the dissipative error related to small time steps. In section 3 we discuss the application to advection diffusion equations for which small time step size is usually required for explicit schemes. The reconstruction procedures with ENO [10] or MUSCL [32] for 1D overlapping cells are discussed in section 4. In section 5, we extend the techniques to 2D and develop a simple diagonal line method. 1D and 2D Numerical examples are shown in section 6.

2 Central Schemes for Scalar Conservation Law in One Space Dimension

Consider 1D conservation law

$$\begin{aligned} &\tfrac{\partial u}{\partial t} + \tfrac{\partial f(u)}{\partial x} = 0, \quad (x,t) \in R \times (0,T) \\ &u(x,0) = u_0(x), \quad x \in R. \end{aligned} \tag{1}$$

Let $\{x_i\}$ be a uniform partition in R, with $\Delta x = x_{i+1} - x_i$. Denote $x_{i+1/2} = \frac{1}{2}(x_i + x_{i+1})$. Let U_i approximate the cell average $\int_{x_{i-1/2}}^{x_{i+1/2}} u(x,t)dx$ and $U_{i+1/2}$

approximate the cell average $\int_{x_i}^{x_{i+1}} u(x,t)dx$. Denote $U_i^n = U_i(t_n)$, $U_{i+1/2}^n = U_{i+1/2}(t_n)$. By applying a MUSCL or ENO reconstruction for the two sets of cell averages, one obtains a function $\mu^n(x)$ which is piece-wise polynomial for cells $\{(x_{i-1/2}, x_{i+1/2}) : i = 0, \pm 1, \pm 2, \cdots\}$ and a function $\nu^n(x)$ which is piece-wise polynomial for cells $\{(x_i, x_{i+1}) : i = 0, \pm 1, \pm 2, \cdots\}$. For conservation purpose of the NT scheme, they should satisfy $\frac{1}{\Delta x}\int_{x_{i-1/2}}^{x_{i+1/2}} \mu^n(x)dx = U_i^n$ and $\frac{1}{\Delta x}\int_{x_i}^{x_{i+1}} \nu^n(x)dx = U_{i+1/2}^n$. Let $\Delta t_n = t_{n+1} - t_n$ be the current time step size, the NT scheme can be written as follows for one time step

$$\begin{aligned} U_i^{n+1} &= \frac{1}{\Delta x}\int_{x_{i-1/2}}^{x_{i+1/2}} \nu^n(x)dx - \frac{\Delta t_n}{\Delta x}[f(\nu^n(x_{i+1/2})) - f(\nu^n(x_{i-1/2}))], \\ U_{i+1/2}^{n+1} &= \frac{1}{\Delta x}\int_{x_i}^{x_{i+1}} \mu^n(x)dx - \frac{\Delta t_n}{\Delta x}[f(\mu^n(x_{i+1})) - f(\mu^n(x_i))]. \end{aligned} \tag{2}$$

Note that this is only first order in time. The higher order time discretization can be obtained by applying the TVD time discretization procedure of Shu and Osher [29]. Kurganov and Tadmor [15] point out that since the numerical dissipation from $\frac{1}{\Delta x}\int_{x_{i-1/2}}^{x_{i+1/2}} \nu^n(x)dx$ does not depend on Δt_n, the accumulative error will depend on $O(1/\Delta t)$, the total number of time steps in the computation. Therefore when Δt is very small, e.g. $\Delta t = O(\Delta x^2)$ for convection diffusion equations, the numerical dissipation becomes large. This is easily seen if $f(u) \equiv 0$, then what the central scheme does is conservative rezoning at every time step, which will smear out the solution with the number of iterations increasing. By choosing the size of the control volume (x_i, x_{i+1}) proportional to Δt as in [15], this $O(1/\Delta t)$ dependence can be removed and by passing the limit as $\Delta t \to 0$, semi-discrete central schemes can be developed. Here we introduce another easy modification of the NT scheme to remove the $O(1/\Delta t)$ dependence of the error taking advantage of the overlapping cell representation U_i^n and $U_{i+1/2}^n$. The idea is to use a time dependent weighted average of $\frac{1}{\Delta x}\int_{x_{i-1/2}}^{x_{i+1/2}} \nu^n(x)dx$ and U_i^n in (2), which will not change the order of accuracy of the scheme. In fact the difference between them is the local dissipation error. Suppose $\Delta t_n \le \Delta \tau_n$ and $\Delta \tau_n$ is an upper bound for the current time step size due to the CFL restriction. The one time step form of the new central scheme can be formulated as follows

$$\begin{aligned} U_i^{n+1} &= \theta(\tfrac{1}{\Delta x}\int_{x_{i-1/2}}^{x_{i+1/2}} \nu^n(x)dx) + (1-\theta)U_i^n - \\ &\qquad \tfrac{\Delta t_n}{\Delta x}[f(\nu^n(x_{i+1/2})) - f(\nu^n(x_{i-1/2}))], \\ U_{i+1/2}^{n+1} &= \theta(\tfrac{1}{\Delta x}\int_{x_i}^{x_{i+1}} \mu^n(x)dx) + (1-\theta)U_{i+1/2}^n - \\ &\qquad \tfrac{\Delta t_n}{\Delta x}[f(\mu^n(x_{i+1})) - f(\mu^n(x_i))], \end{aligned} \tag{3}$$

where $\theta = \Delta t_n/\Delta\tau_n$. Note that when $\theta = 1$, it becomes the NT scheme represented on overlapping cells. One can also obtain the following semi-discrete form by moving U_i^n and $U_{i+1/2}^n$ to the left hand side and multiplying both side by $\frac{1}{\Delta t_n}$, then passing the limit as $\Delta t_n \to 0$

$$\begin{aligned} \tfrac{d}{dt}U_i(t_n) &= \tfrac{1}{\Delta\tau_n\Delta x}\int_{x_{i-1/2}}^{x_{i+1/2}} \nu^n(x)dx - \tfrac{1}{\Delta\tau_n}U_i^n - \\ &\qquad \tfrac{1}{\Delta x}[f(\nu^n(x_{i+1/2})) - f(\nu^n(x_{i-1/2}))], \\ \tfrac{d}{dt}U_{i+1/2}(t_n) &= \tfrac{1}{\Delta\tau_n\Delta x}\int_{x_i}^{x_{i+1}} \mu^n(x)dx - \tfrac{1}{\Delta\tau_n}U_{i+1/2}^n - \\ &\qquad \tfrac{1}{\Delta x}[f(\mu^n(x_{i+1})) - f(\mu^n(x_i))]. \end{aligned} \tag{4}$$

Note that this semi-discrete form doesn't need to explicitly evaluate the jump values of $\nu^n(x)$ and $\mu^n(x)$ across their respective cell edges (which is one of the features of the NT scheme), thus is more convenient to use for finite volume representations in multi space dimension with unstructured mesh. See Figures 1, 2 and 3. To study the non-oscillatory property of the scheme (3), denote $TV\{U_i^{n+1}\} = \sum_i |U_{i+1}^{n+1} - U_i^{n+1}|$ as the total variation of U_i^{n+1}. We say a scheme is TVD from time t_n to t_{n+1} if

$$\max\{TV\{U_i^{n+1}\}, TV\{U_{i+1/2}^{n+1}\}\} \le \max\{TV\{U_i^n\}, TV\{U_{i+1/2}^n\}\} < \infty.$$

We have the following theorem.

Theorem 1 *Let the schemes (2) and (3) start from the same time t_n with the same initial values U_i^n and $U_{i+1/2}^n$. If the scheme (2) is TVD from time step t_n to $t_n+\Delta\tau_n$, then the scheme (3) is also TVD from time t_n to $t_n+\Delta t_n$, for any $\Delta t_n \in [0, \Delta\tau_n]$.*

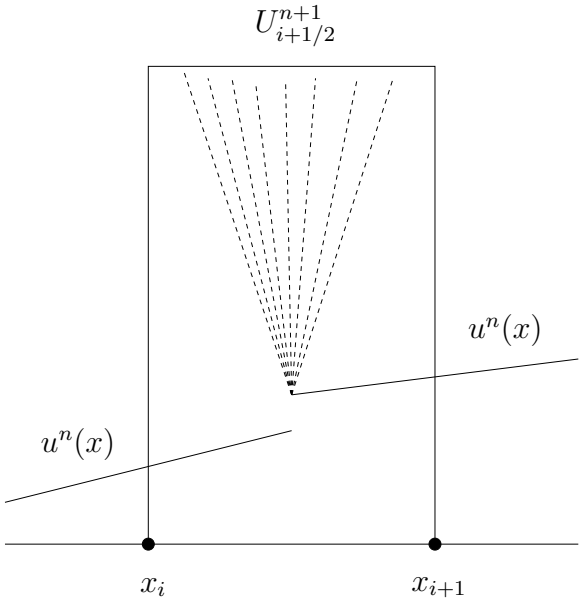

Figure 1: Nessyahu and Tadmor's central scheme

Proof: Note that the first equation of (3) can be rewritten as

$$\begin{aligned} U_i^{n+1} &= \theta\{\tfrac{1}{\Delta x}\int_{x_{i-1/2}}^{x_{i+1/2}} \nu^n(x)dx - \tfrac{\Delta\tau_n}{\Delta x}[f(\nu^n(x_{i+1/2}) - f(\nu^n(x_{i-1/2})]\}+ \\ & (1-\theta)U_i^n. \end{aligned}$$

This is a convex combination of the U_i^{n+1} calculated from the scheme (2) with time step size $\Delta\tau_n$ and U_i^n. Since the scheme (2) is TVD for time step size $\Delta\tau_n$, therefore the U_i^{n+1} computed by the scheme (3) satisfies $TV\{U_i^{n+1}\} \leq \max\{TV\{U_i^n\}, TV\{U_{i+1/2}^n\}\} < \infty$. Similarly from the second equation of (3) we conclude that $U_{i+1/2}^{n+1}$ computed by (3) satisfies

$$TV\{U_{i+1/2}^{n+1}\} \leq \max\{TV\{U_i^n\}, TV\{U_{i+1/2}^n\}\}.$$

The proof is complete. □

Remark. The proof follows closely the strategy used in [29]. If we change the definition of total variation to $TV\{U_i^{n+1}\} = \sum_{2i=0,\pm1,\pm2,\cdots} |U_i^{n+1} - U_{i-1/2}^{n+1}|$, Theorem 1 is still true following a similar argument. These two versions of the theorems provide us some insights into two reconstruction procedures:

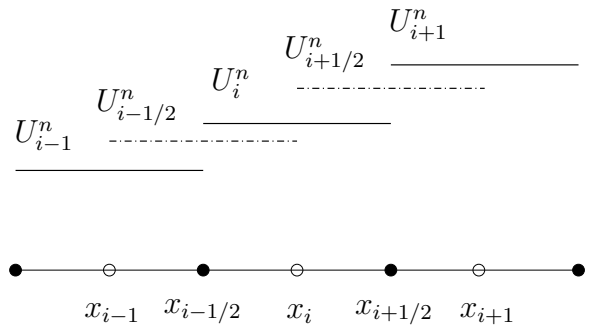

Figure 2: One dimensional overlapping cells

one is standard to reconstruct for the two classes of cell averages $\{U^n_i : i = 0, \pm1, \pm2, \cdots\}$ and $\{U^n_{i+1/2} : i = 0, \pm1, \pm2, \cdots\}$ separately; the other mixes the two classes in the reconstruction. We will discuss more for the second one in the following sections.

Note that in (3),

$$\theta(\tfrac{1}{\Delta x}\int_{x_{i-1/2}}^{x_{i+1/2}} \nu^n(x)dx) + (1-\theta)U^n_i$$

$$= U^n_i + \tfrac{\Delta t_n}{\Delta \tau_n}(\tfrac{1}{\Delta x}\int_{x_{i-1/2}}^{x_{i+1/2}} \nu^n(x)dx - U^n_i).$$

and $\Delta\tau_n = O(\Delta x)$ is due to the CFL restriction for the NT scheme. Therefore the local dissipative error now has a factor of Δt_n and the cumulative error will not be degenerated by choosing very small Δt_n. It will be interesting to see the first order correspondence of (3) relative to the Lax-Friedrich scheme,

$$\begin{aligned} U^{n+1}_i &= \theta\tfrac{U^n_{i-1/2}+U^n_{i+1/2}}{2} + (1-\theta)U^n_i - \tfrac{\Delta t_n}{\Delta x}\{f(U^n_{i+1/2}) - f(U^n_{i-1/2})\} \\ &= U^n_i - \tfrac{\Delta t_n}{\Delta x/2}\{F^n_{i+1/4} - F^n_{i-1/4}\}, \end{aligned}$$

where $F^n_{i+1/4} = \frac{1}{2}\{f(U^n_i) + f(U^n_{i+1/2})\} + \frac{\Delta x/2}{2\Delta\tau_n}(U^n_i - U^n_{i+1/2})$. This is the Lax-Friedrich flux with diffusive coefficient $\frac{\Delta x}{2\Delta\tau_n}$ (see e.g. Shu [28]), which should be chosen to be larger than $\max_u |f'(u)|$ in order for the flux $F^n_{i+1/4}$ to be a monotone flux. Therefore the modified Lax-Friedrich scheme can be viewed as the Godunov scheme with an approximate Lax-Friedrich Riemann solver.

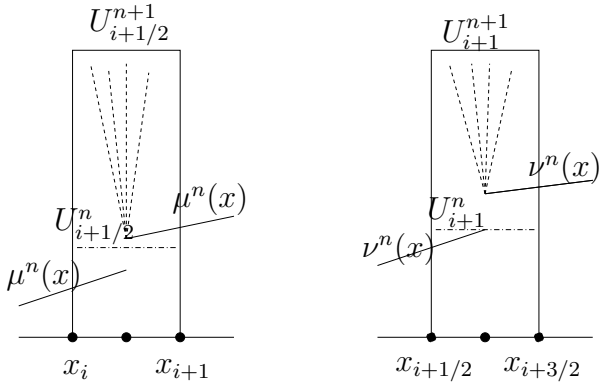

Figure 3: Central scheme on overlapping cells allows a convex combination of the cell averages

When $\theta = 1$, *i.e.* $\Delta t_n = \Delta\tau_n$, it becomes the original non-staggered Lax-Friedrich scheme.

Following [29], a predictor-corrector time discretization procedure is TVD provided that the two one-step schemes in the procedure are both TVD, therefore the fully discretized second order version of the scheme (3) can be obtained conveniently as follows.

Predictor:

$$\tilde{U}^{n+1}_i = \frac{\theta}{\Delta x}\int_{x_{i-1/2}}^{x_{i+1/2}} \nu^n(x)dx + (1-\theta)U^n_i - \frac{\Delta t_n}{\Delta x}[f(\nu^n(x_{i+1/2})) - f(\nu^n(x_{i-1/2}))],$$

$$\tilde{U}^{n+1}_{i+1/2} = \frac{\theta}{\Delta x}\int_{x_i}^{x_{i+1}} \mu^n(x)dx + (1-\theta)U^n_{i+1/2} - \frac{\Delta t_n}{\Delta x}[f(\mu^n(x_{i+1})) - f(\mu^n(x_i))]. \tag{5}$$

Corrector:

$$\hat{U}^{n+2}_i = \frac{\theta}{\Delta x}\int_{x_{i-1/2}}^{x_{i+1/2}} \tilde{\nu}^{n+1}(x)dx + (1-\theta)\tilde{U}^{n+1}_i - \frac{\Delta t_n}{\Delta x}[f(\tilde{\nu}^{n+1}(x_{i+1/2})) - f(\tilde{\nu}^{n+1}(x_{i-1/2}))],$$

$$\hat{U}^{n+2}_{i+1/2} = \frac{\theta}{\Delta x}\int_{x_i}^{x_{i+1}} \tilde{\mu}^{n+1}(x)dx + (1-\theta)\tilde{U}^{n+1}_{i+1/2} - \frac{\Delta t_n}{\Delta x}[f(\tilde{\mu}^{n+1}(x_{i+1})) - f(\tilde{\mu}^{n+1}(x_i))]. \tag{6}$$

Average:

$$\begin{aligned} U^{n+1}_i &= \tfrac{1}{2}\{U^n_i + \hat{U}^{n+2}_i\}, \\ U^{n+1}_{i+1/2} &= \tfrac{1}{2}\{U^n_{i+1/2} + \hat{U}^{n+2}_{i+1/2}\}. \end{aligned} \tag{7}$$

Remark. In some high order TVD Runge-Kutta methods of [29], the time step size cannot have CFL factor 1 which requires that θ has to be adjusted correspondingly. For example, in one form of the 4th order TVD Runge-Kutta method, the CFL factor is 2/3, which implies that Δt_n should satisfy $\Delta t_n \leq 2/3\Delta\tau_n$ when applying it to the semi-discrete scheme (4).

3 Central Schemes for Convection Diffusion Equation in One Space Dimension

Consider the convection diffusion equation

$$\begin{aligned} &\tfrac{\partial u}{\partial t} + \tfrac{\partial f(u)}{\partial x} = \tfrac{\partial}{\partial x}(a(u,x,t)\tfrac{\partial u}{\partial x}), \quad (x,t) \in R \times (0,T) \\ &u(x,0) = u_0(x), \qquad\qquad\qquad\quad x \in R, \end{aligned} \tag{8}$$

where $a(u,x,t) \geq 0$. Following the work of Kurganov and Tadmor [15], we can discretize equation (8) as follows

$$\begin{aligned} U_i^{n+1} &= \theta(\tfrac{1}{\Delta x}\int_{x_{i-1/2}}^{x_{i+1/2}} \nu^n(x)dx) + (1-\theta)U_i^n - \\ &\quad \tfrac{\Delta t_n}{\Delta x}[f(\nu^n(x_{i+1/2})) - f(\nu^n(x_{i-1/2}))] \\ &\quad + \tfrac{\Delta t_n}{\Delta x}[a(U_{i+1/2}^n, x_{i+1/2}, t_n)\tfrac{U_{i+1}^n - U_i^n}{\Delta x} - a(U_{i-1/2}^n, x_{i-1/2}, t_n)\tfrac{U_i^n - U_{i-1}^n}{\Delta x}], \\ U_{i+1/2}^{n+1} &= \theta(\tfrac{1}{\Delta x}\int_{x_i}^{x_{i+1}} \mu^n(x)dx) + (1-\theta)U_{i+1/2}^n - \\ &\quad \tfrac{\Delta t_n}{\Delta x}[f(\mu^n(x_{i+1})) - f(\mu^n(x_i))] \\ &\quad + \tfrac{\Delta t_n}{\Delta x}[a(U_{i+1}^n, x_{i+1}, t_n)\tfrac{U_{i+3/2}^n - U_{i+1/2}^n}{\Delta x} - a(U_i^n, x_i, t_n)\tfrac{U_{i+1/2}^n - U_{i-1/2}^n}{\Delta x}], \end{aligned} \tag{9}$$

where $\theta = \Delta t_n/\Delta\tau_n$, $\Delta\tau_n$ is maximum time step size determined by the CFL restriction for the hyperbolic part of the equation (8), $\frac{\partial u}{\partial t} + \frac{\partial f(u)}{\partial x} = 0$.

We have the following stability theorem.

Theorem 2 *Let the schemes (2) and (9) start from the same time t_n with the same initial values U_i^n and $U_{i+1/2}^n$. If the scheme (2) is TVD from time step*

t_n to $t_n+\Delta\tau_n$, then the scheme (9) is also TVD from time t_n to $t_n+\Delta t_n$, for any $\Delta t_n \le \frac{\Delta\tau_n\Delta x^2}{\Delta x^2+2a_n\Delta\tau_n}$, with $a_n = \sup\{a(U^n_{i+1}, x_{i+1}, t_n), a(U^n_{i+1/2}, x_{i+1/2}, t_n) : i = 0, \pm1, \pm2, \cdots\}$.

Proof: Note that the first equation of (9) can be rewritten as

$$\begin{aligned} U_i^{n+1} &= \theta\{\tfrac{1}{\Delta x}\int_{x_{i-1/2}}^{x_{i+1/2}} \nu^n(x)dx - \tfrac{\Delta\tau_n}{\Delta x}[f(\nu^n(x_{i+1/2})) - f(\nu^n(x_{i-1/2}))]\}+ \\ &\quad (1-\theta-\tfrac{(a(U^n_{i+1/2},x_{i+1/2},t_n)+a(U^n_{i-1/2},x_{i-1/2},t_n))\Delta t_n}{\Delta x^2})U_i^n+ \\ &\quad \tfrac{\Delta t_n a(U^n_{i-1/2},x_{i-1/2},t_n)}{\Delta x^2}U^n_{i-1} + \tfrac{\Delta t_n a(U^n_{i+1/2},x_{i+1/2},t_n)}{\Delta x^2}U^n_{i+1}. \end{aligned}$$

The condition of the theorem will ensure that the coefficient of U_i^n is non-negative. Therefore U_i^{n+1} in (9) is a convex combination of the U_i^{n+1} calculated from the scheme (2) with time step size $\Delta\tau_n$, U_i^n, U^n_{i-1} and U^n_{i+1}. Since the scheme (2) is TVD for the time step size $\Delta\tau_n$, therefore the U_i^{n+1} computed by the scheme (9) satisfies $TV\{U_i^{n+1}\} \le \max\{TV\{U_i^n\}, TV\{U^n_{i+1/2}\}\} < \infty$. Similarly for the second equation of (9) and the proof is complete. □

4 Reconstruction in One Space Dimension

For separation of the two classes of the cells, we will denote $V_i^n = U^n_{i+1/2}$, $i = 0, \pm1, \pm2, \cdots$ with their supporting cells $D_i = (x_i, x_{i+1})$. Correspondingly, the cells supporting U_i^n will be denoted as $C_i = (x_{i-1/2}, x_{i+1/2})$. The most straight forward way of reconstruction is to do it for cell class $\{U_i\}$ and $\{V_i\}$ separately. Since there is no overlapping of cells within $\{U_i\}$ or within $\{V_i\}$, standard reconstruction methods, e.g. MUSCL, ENO etc, can be used.

4.1 High Order Reconstruction Using Combined Cells

The interesting question is what happens if we combine cells $\{U_i\}$ and $\{V_i\}$ in the reconstruction. Let's consider for example the reconstruction for the cell with cell average U_i^n. For simplicity we only use the information from overlapping cells adjacent to cell C_i or with overlap to C_i, see Fig. 4. A 4th order polynomial can be written as

$$p_4(x) = a_0 + a_1(x-x_i) + a_2(x-x_i)^2 + a_3(x-x_i)^3 + a_4(x-x_i)^4.$$

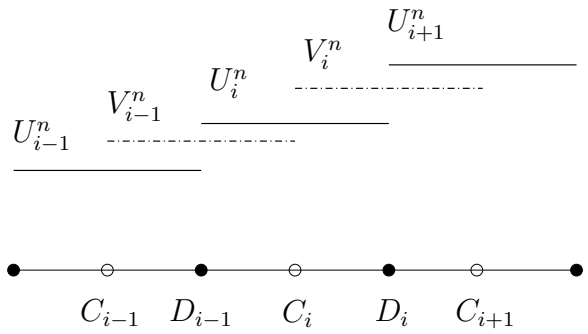

Figure 4: One dimension overlapping cells with change of notation

Adapting the strategy of Abgrall [3] to overlapping cells, we may simply let $\frac{1}{\Delta x}\int_{C_j} p_4(x)dx = U^n_j$, $j = i, i \pm 1$ and $\frac{1}{\Delta x}\int_{D_j} p_4(x)dx = V^n_j$, $j = i, i-1$ to find the coefficients. For example,

$$\begin{array}{rcl} a_0 &=& \frac{1}{30}[U^n_{i-1} + U^n_{i+1} + 46U^n_i - 9(V^n_{i-1} + V^n_i)], \\ a_1 &=& \frac{1}{3\Delta x}[U^n_{i-1} - U^n_{i+1} - 5(V^n_{i-1} - V^n_i)], \\ a_2 &=& -\frac{1}{2\Delta x^2}[U^n_{i-1} + U^n_{i+1} + 14U^n_i - 8(V^n_{i-1} + V^n_i)], \\ a_3 &=& -\frac{2}{3\Delta x^3}[U^n_{i-1} - U^n_{i+1} - 2(V^n_{i-1} - V^n_i)], \\ a_4 &=& \frac{2}{3\Delta x^4}[U^n_{i-1} + U^n_{i+1} + 6U^n_i - 4(V^n_{i-1} + V^n_i)]. \end{array} \tag{10}$$

There are many possible 3rd order polynomials

$$p_3(x) = a_0 + a_1(x - x_i) + a_2(x - x_i)^2 + a_3(x - x_i)^3$$

defined in this stencil of overlapping cells. For example, a symmetric one is defined by enforcing the cell averages at cells C_i and $C_{i-1} \cup C_i \cup C_{i+1}$ which gives

$$\begin{array}{rcl} a_0 &=& -\frac{1}{24}[U^n_{i-1} + U^n_{i+1} - 26U^n_i], \\ a_2 &=& \frac{1}{2\Delta x^2}[U^n_{i-1} + U^n_{i+1} - 2U^n_i], \end{array} \tag{11}$$

Then use least square fit (see e.g., Barth and Frederickson [4]) on cells D_{i-1} and D_i, which gives the rest of the two coefficients.

$$\begin{array}{rcl} a_1 &=& \frac{1}{3\Delta x}[(U^n_{i-1} - U^n_{i+1}) - 5(V^n_{i-1} - V^n_i)], \\ a_3 &=& \frac{4}{3\Delta x^3}[-\frac{1}{2}(U^n_{i-1} - U^n_{i+1}) + (V^n_{i-1} - V^n_i)]. \end{array} \tag{12}$$

In order to verify the accuracy of the reconstructions using combined overlapping cells, we build a test scheme as follows.

The simplest way to take advantage of these locally constructed high order polynomials is to combine them with a low order polynomial, using proper smooth indicators to turn on the high order polynomial in a smooth region and turn off it in a non-smooth region. This follows the works of Liu, Osher and Chan [24], Liu and Tadmor [25], Levy, Puppo and Russo [21] and Kurganov and Petrova[17]. For example, let $p_l(x)$ be the linear polynomial having the given cell averages in cells C_{i-1} and C_i and $p_r(x)$ be the linear polynomial having the given cell averages in cells C_i and C_{i+1}. Let $p(x) = w_3 p_3(x) + w_l p_l(x) + w_r p_r(x)$ where w_3, w_l, w_r are some non-negative weights satisfying $w_3 + w_l + w_r = 1$, thus $p(x)$ also conserves the cell averages. In order to determine the weights, let IS_3, IS_l, IS_r be the corresponding smooth indicators so that $IS_3 = 1/[(\Delta x a_3)^4 + \epsilon]$, $IS_l = 1/[IS_3 + (p_l')^4 + \epsilon]$, and $IS_r = 1/[IS_3 + (p_r')^4 + \epsilon]$. Let $w = IS_3 + IS_l + IS_r$, then finally let $w_3 = IS_3/w$, $w_l = IS_l/w$, $w_r = IS_r/w$. It is easy to verify that these weights satisfies the ENO principle as defined in Liu, Osher and Chan [24] in the sense that in smooth regions they satisfy the accuracy requirement while in non-smooth regions $w_3 = O(\Delta x^4)$, enough to control $p_3(x)$, and w_l and w_r will shift the weights to the flatter linear polynomial.

Remark. The accuracy test for this scheme is included which helps verify the accuracy of the reconstructions for combined overlapping cells. Similar reconstruction using $p_5(x)$ has also been done with expected accuracy on smooth test problems. These simple reconstructions also seem to work fine for various test problems for Euler equation.

4.2 Compact Quadratic ENO Reconstruction Using Combined Overlapping Cells

Note that in Fig. 4, there affords a full ENO stencil for quadratic polynomials. In order to obtain a quadratic polynomial

$$p_2(x) = a_0 + a_1(x - x_i) + a_2(x - x_i)^2$$

in cell C_i, there are 3 possible stencils of overlapping cells to choose from, namely, $\{C_{i-1}, D_{i-1}, C_i\}$, $\{D_{i-1}, C_i, D_i\}$ or $\{C_i, D_i, C_{i+1}\}$. Viewing the cell averages as point values at their respective cell centers, The Newton divided difference (Harten *et. al.*[10]) can be used as the smooth indicator to pick one stencil which contains the smoothest data. For example, if the stencil

$\{D_{i-1}, C_i, D_i\}$ is chosen, then the quadratic polynomial can be constructed by letting $\frac{1}{\Delta x}\int_{D_{i-1}} p_2(x)dx = V_{i-1}^n$, $\frac{1}{\Delta x}\int_{C_i} p_2(x)dx = U_i^n$ and $\frac{1}{\Delta x}\int_{D_i} p_2(x)dx = V_i^n$. For example, the formula for the coefficients of p_2, given the cell averages of p_2, A_0, A_1, A_2, at 3 different cells of size h and cell center positions $x_i + \xi_0, x_i + \xi_1, x_i + \xi_2$ can be written as follows

$$\begin{aligned} a_2 &= \tfrac{1}{\xi_2-\xi_1}[\tfrac{A_2-A_0}{\xi_2-\xi_0} - \tfrac{A_1-A_0}{\xi_1-\xi_0}], \\ a_1 &= \tfrac{A_1-A_0}{\xi_1-\xi_0} - (\xi_1+\xi_0)a_2, \\ a_0 &= A_0 - \xi_0 a_1 - (\xi_0^2 + \tfrac{h^2}{12})a_2. \end{aligned} \tag{13}$$

Remark. The quadratic ENO Reconstruction using combined overlapping cells for (3) is tested for many problems in this paper and provides good robustness and resolution. It is also used for a compact diagonal line method for 2D.

4.3 Linear ENO and MUSCL Reconstructions Using Combined Overlapping Cells

Following the previous discussion, It is straight forward to apply the second order ENO or MUSCL linear reconstructions for cell C_i using only the closest overlapping cells, D_{i-1} and D_i, see Fig. 4. For a volume conserving linear polynomial $p_2(x) = a_0 + a_1(x - x_i)$ with $a_0 = U_i^n$, the only thing left is to determine the slope a_1 using information from cells D_{i-1} and D_i. The numerical experiments show that these combined local reconstructions produce better resolution than those reconstructed separately for each class of cells.

5 Two Space Dimension

Consider the system of conservation laws in two space dimension

$$\frac{\partial u}{\partial t} + \frac{\partial f(u)}{\partial x} + \frac{\partial g(u)}{\partial y} = 0, \quad (x, y, t) \in R^2 \times (0, T). \tag{14}$$

Assuming a uniform rectangular mesh with mesh size $\Delta x \times \Delta x$, and cell center positions $\mathbf{x}_{i,j} = (x_i, y_j) = (i\Delta x, j\Delta x)$. Let $U_{i,j}^n$ denote the cell average of u in

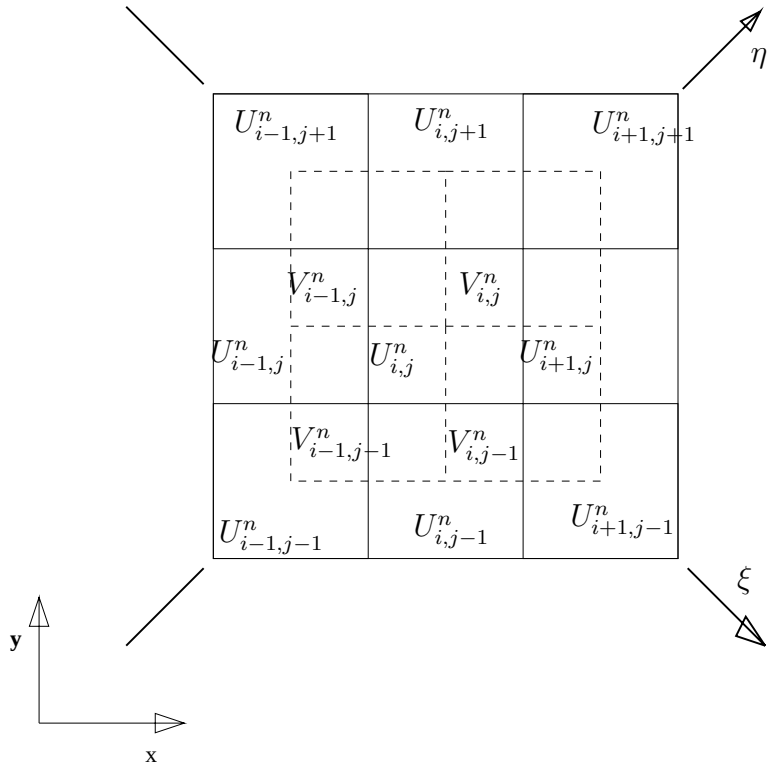

Figure 5: Two dimensional (staggered) overlapping cells

the cell centered at $\mathbf{x}_{i,j}$ at time level t_n. The most common staggered mesh would be to shift the original mesh along the vector $(\frac{1}{2}\Delta x, \frac{1}{2}\Delta x)$, thus a cell centered at $\mathbf{x}_{i,j}$ will be shift to a new cell centered at $\mathbf{y}_{i,j} = \mathbf{x}_{i,j} + (\frac{1}{2}\Delta x, \frac{1}{2}\Delta x)$. By assigning the cell averages $V^n_{i,j}$ of u to the new cell at the same time level t_n, we obtain overlapping cell average representation of the function u. See Fig. 5, the original cells are bounded by solid lines while the shifted staggered cells are bounded by dashes. To simplify the terminology, we will frequently call the original cell centered at $\mathbf{x}_{i,j}$ the cell of $U^n_{i,j}$ and call the overlapping cell centered at $\mathbf{y}_{i,j}$ the cell of $V^n_{i,j}$.

Suppose in each cell we have a reconstructed polynomial which conserves the cell average. Let $\mu^n(x, y)$ be a piecewise polynomial reconstructed on the

original cells of $U^n_{i,j}$ s.t.

$$\frac{1}{\Delta x^2}\int_{\text{cell of } U_{i,j}} \mu^n(x,y)dxdy = U^n_{i,j},$$

and $\nu^n(x,y)$ be the piecewise polynomial reconstructed on the shifted staggered cells of $V^n_{i,j}$ s.t.

$$\frac{1}{\Delta x^2}\int_{\text{cell of } V_{i,j}} \nu^n(x,y)dxdy = V^n_{i,j}.$$

We can write the 2D central scheme analogous to (3) as follows

$$\begin{aligned} U^{n+1}_{i,j} &= \theta(\tfrac{1}{\Delta x^2}\textstyle\int_{\text{cell of } U_{i,j}} \nu^n dxdy) + (1-\theta)U^n_{i,j} - \\ &\qquad \tfrac{\Delta t_n}{\Delta x^2}\textstyle\int_{\partial(\text{cell of } U^n_{i,j})}(f(\nu^n), g(\nu^n))\cdot \mathbf{n} ds, \\ V^{n+1}_{i,j} &= \theta(\tfrac{1}{\Delta x^2}\textstyle\int_{\text{cell of } V_{i,j}} \mu^n dxdy) + (1-\theta)V^n_{i,j} - \\ &\qquad \tfrac{\Delta t_n}{\Delta x^2}\textstyle\int_{\partial(\text{cell of } V^n_{i,j})}(f(\mu^n), g(\mu^n))\cdot \mathbf{n} ds. \end{aligned} \tag{15}$$

where $\mathbf{n}$ denotes unit outer normal of the corresponding cell boundary, $\theta = \Delta t_n/\Delta\tau_n \le 1$, $\Delta t_n = t_{n+1} - t_n$ is the actual time step size, $\Delta\tau_n$ is determined by the CFL restriction of the NT scheme. The evaluation of the fluxes integrated along the cell boundary can be evaluated with the quadrature, see e.g. Levy, Puppo and Russo [22]. One can also obtain a semi-discrete form by moving $U^n_{i,j}$ and $V^n_{i,j}$ to the left hand side and multiplying both side by $\frac{1}{\Delta t_n}$, then passing the limit as $\Delta t_n \to 0$. Therefore the TVD Runge-Kutta methods of Shu and Osher [29] can be used to obtain a fully discretized scheme with suitable order of accuracy in time.

As in the 1D case, the reconstruction can be done for each class of cells separately or for combined overlapping cells. The second order reconstruction for combined overlapping cells is particularly simple. For example, for the cell of $U^n_{i,j}$, the volume conserving linear polynomial can be written as

$$p_1(\mathbf{x}) = U^n_{i,j} + \mathbf{a}_1\cdot(\mathbf{x} - \mathbf{x}_{i,j}),$$

where $\mathbf{x} = (x,y)$. The gradient $\mathbf{a}_1$ can be determined by choosing two smoothest cells from the cells of $U^n_{i-1,j}$, $V^n_{i-1,j}$, $U^n_{i,j+1}$, $V^n_{i,j}$, $U^n_{i+1,j}$, $V^n_{i,j-1}$, $U^n_{i,j-1}$

or $V^n_{i-1,j-1}$, or choose two only from the overlapping cells of $V^n_{i-1,j}$, $V^n_{i,j}$, $V^n_{i,j-1}$ or $V^n_{i-1,j-1}$. See Fig. 5.

By introducing overlapping cell averages for the staggered mesh at each time level, finite volume implementation with regular or irregular staggered mesh becomes easier with the TVD Runge-Kutta time discretization methods of [29]. Also notice that the semi-discrete form of (15) does not contain any explicit evaluation of the jump values at cell boundaries.

5.1 A Third Order Diagonal Line Method in 2D

In order to take full advantage of the information on overlapping cells as in Fig. 5, an efficient line by line reconstruction would be to go along the diagonal direction since each of the the diagonal lines passes through the centroid of 5 overlapping cells adjacent to cell of $U^n_{i,j}$. We can set a local coordinate ξ, η as in Fig. 5, which is a rigid rotation of the x, y coordinate clock-wisely $\pi/4$ angle followed by a shift to the cell center. The (ξ, η) coordinate for a fixed point with coordinate (x, y) is

$$\begin{array}{rcl} \xi &=& \frac{\sqrt{2}}{2}(x - x_i) - \frac{\sqrt{2}}{2}(y - y_j), \\ \eta &=& \frac{\sqrt{2}}{2}(x - x_i) + \frac{\sqrt{2}}{2}(y - y_j). \end{array} \tag{16}$$

The conservation laws (14) can be written as

$$\frac{\partial u}{\partial t} + \frac{\partial F(u)}{\partial \xi} + \frac{\partial G(u)}{\partial \eta} = 0, \tag{17}$$

where $F(u) = \frac{\sqrt{2}}{2} f(u) - \frac{\sqrt{2}}{2} g(u)$, $G(u) = \frac{\sqrt{2}}{2} f(u) + \frac{\sqrt{2}}{2} g(u)$.

Now assume the solution is piecewise constant (the cell averages) represented in the 2D overlapping cells. If we look at the cross-section of this piecewise constant solution on the ξ-axis, we obtain a one dimensional piecewise constant solution on the overlapping cells along ξ-axis, see the upper graph of Fig. 6. Viewing these constants as the corresponding cell averages of the solution on the 1D overlapping cells along ξ-axis, we can then apply the reconstruction procedures discussed in previous sections to obtain a local 1D polynomial $\mu^n_{i,j}(\xi)$ for the cell of $U^n_{i,j}$ along ξ-direction. Note that there are exactly 5 overlapping cells along ξ-axis, thus the quadratic ENO reconstruction discussed in Section 4.2 can be applied here to construct the second order

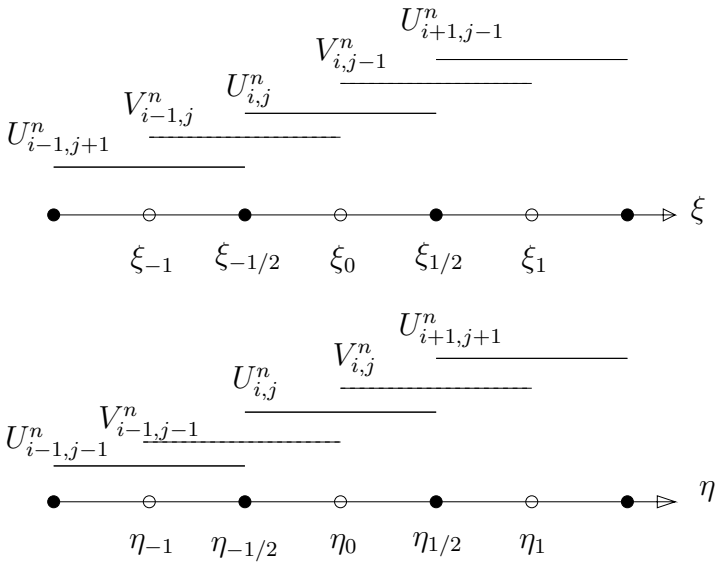

Figure 6: Overlapping cells along two diagonal lines

polynomial $\mu^n_{i,j}(\xi)$ on interval $(\xi_{-1/2}, \xi_{1/2})$ within the cell of $U^n_{i,j}$. Note that we are going to set such a local coordinate for every cell. The corresponding parameters in the upper graph of Fig. 6 are $\xi_k = k\Delta\xi$ with $\Delta\xi = \sqrt{2}\Delta x$. It is important to recognize the scale difference between Δx and $\Delta\xi$ because it will affect the CFL restriction which will be discussed in a moment. Similarly looking at the cross-section of the solution along the η-axis we obtain a 1D piecewise constant solution defined as in the lower graph of Fig. 6 with parameters $\eta_k = k\Delta\xi$, thus we can apply the quadratic ENO reconstruction to obtain a quadratic polynomial $\tilde{\mu}^n_{i,j}(\eta)$ defined on the interval $(\eta_{-1/2}, \eta_{1/2})$ within the cell of $U^n_{i,j}$. We can apply the same procedure for the cell of $V^n_{i,j}$ to obtain two local quadratic polynomial $\nu^n_{i,j}(\xi)$ defined on its local ξ-axis and $\tilde{\nu}^n_{i,j}(\eta)$ defined on its local η-axis.

Following the work of Kurganov and Tadmor [15], we can write the semi-discrete 2D scheme based on (4) as follows

$$\begin{array}{rcl} \frac{d}{dt}U_{i,j}(t_n) & = & -D_\xi F(V^n)_{i,j} - D_\eta G(V^n)_{i,j}, \\ \frac{d}{dt}V_{i,j}(t_n) & = & -D_\xi F(U^n)_{i,j} - D_\eta G(U^n)_{i,j}, \end{array} \tag{18}$$

where $-D_\xi F(V^n)_{i,j}$ is an approximation to $-\frac{\partial F(u)}{\partial \xi}$ at the cell centroid of

the cell of $U^n_{i,j}$ which is a correspondence to the right hand side of the first equation of the 1D semi-discrete central scheme (4). It is similar for the others. These flux derivatives can be written down explicitly as follows

$$\begin{aligned} -D_\xi F(V^n)_{i,j} &= \tfrac{1}{\Delta\tau_n\Delta\xi}\{\textstyle\int_0^{\frac{1}{2}\Delta\xi}\nu^n_{i-1,j}(\xi)d\xi + \int_{-\frac{1}{2}\Delta\xi}^0 \nu^n_{i,j-1}(\xi)d\xi\}- \\ &\quad \tfrac{1}{\Delta\tau_n}U^n_{i,j} - \tfrac{1}{\Delta\xi}[F(\nu^n_{i,j-1}(0)) - F(\nu^n_{i-1,j}(0))], \\ -D_\eta G(V^n)_{i,j} &= \tfrac{1}{\Delta\tau_n\Delta\xi}\{\textstyle\int_0^{\frac{1}{2}\Delta\xi}\tilde\nu^n_{i-1,j-1}(\eta)d\eta + \int_{-\frac{1}{2}\Delta\xi}^0 \tilde\nu^n_{i,j}(\eta)d\eta\}- \\ &\quad \tfrac{1}{\Delta\tau_n}U^n_{i,j} - \tfrac{1}{\Delta\xi}[G(\tilde\nu^n_{i,j}(0)) - G(\tilde\nu^n_{i-1,j-1}(0))], \end{aligned} \tag{19}$$

and

$$\begin{aligned} -D_\xi F(U^n)_{i,j} &= \tfrac{1}{\Delta\tau_n\Delta\xi}\{\textstyle\int_0^{\frac{1}{2}\Delta\xi}\mu^n_{i,j+1}(\xi)d\xi + \int_{-\frac{1}{2}\Delta\xi}^0 \mu^n_{i+1,j}(\xi)d\xi\}- \\ &\quad \tfrac{1}{\Delta\tau_n}V^n_{i,j} - \tfrac{1}{\Delta\xi}[F(\mu^n_{i+1,j}(0)) - F(\mu^n_{i,j+1}(0))], \\ -D_\eta G(U^n)_{i,j} &= \tfrac{1}{\Delta\tau_n\Delta\xi}\{\textstyle\int_0^{\frac{1}{2}\Delta\xi}\tilde\mu^n_{i,j}(\eta)d\eta + \int_{-\frac{1}{2}\Delta\xi}^0 \tilde\mu^n_{i+1,j+1}(\eta)d\eta\}- \\ &\quad \tfrac{1}{\Delta\tau_n}V^n_{i,j} - \tfrac{1}{\Delta\xi}[G(\tilde\mu^n_{i+1,j+1}(0)) - G(\tilde\mu^n_{i,j}(0))]. \end{aligned} \tag{20}$$

Remark on the CFL Restriction. We can write the semi-discrete 2D method into fully discrete form with forward Euler time discretization. For example, the first equation of (18) can be written as

$$\begin{aligned} U^{n+1}_{i,j} &= \theta\cdot\{\tfrac{1}{\Delta\xi}[\textstyle\int_0^{\frac{1}{2}\Delta\xi}\nu^n_{i-1,j}(\xi)d\xi + \int_{-\frac{1}{2}\Delta\xi}^0 \nu^n_{i,j-1}(\xi)d\xi]- \\ &\quad \tfrac{\Delta\tau_n}{\Delta\xi}[F(\nu^n_{i,j-1}(0)) - F(\nu^n_{i-1,j}(0))]\}+ \\ &\quad \theta\cdot\{\tfrac{1}{\Delta\xi}[\textstyle\int_0^{\frac{1}{2}\Delta\xi}\tilde\nu^n_{i-1,j-1}(\eta)d\eta + \int_{-\frac{1}{2}\Delta\xi}^0 \tilde\nu^n_{i,j}(\eta)d\eta]- \\ &\quad \tfrac{\Delta\tau_n}{\Delta\xi}[G(\tilde\nu^n_{i,j}(0)) - G(\tilde\nu^n_{i-1,j-1}(0))]\}+ \\ &\quad (1-2\theta)\cdot U^n_{i,j}, \end{aligned} \tag{21}$$

where $\theta = \Delta t_n/\Delta\tau_n \le 1$, $\Delta t_n = t_{n+1} - t_n$ is the time step size for the forward Euler discretization. On each diagonal direction the line method can afford a CFL factor (w.r.t. $\Delta\xi$) at most 0.5 ensuring that the center Riemann fan doesn't reach the cell boundary, which is the essential property of the 1D NT scheme. Since $\Delta\xi = \sqrt{2}\Delta x$, this translates to a CFL factor of no more than $\sqrt{2}/2$ for choosing $\Delta\tau_n$. But for this line method, we may NOT be able to choose θ up to 1 any more. In fact, the coefficient in front of $U^n_{i,j}$ is $1 - 2\theta$. Therefore in order to make sure the combination is convex (following a similar argument in the proof of Theorem 1) we need $1 - 2\theta \ge 0$, which implies $\theta \le \frac{1}{2}$ or $\Delta t_n \le \frac{1}{2}\Delta\tau_n$. Note that this implies the actual CFL factor for choosing Δt_n is at most $\sqrt{2}/4$ w.r.t. Δx, but surprisingly we can choose a larger $\Delta\tau_n$ than the 1D central scheme ! This gives us a larger range of control of the dissipation. Remember Δt_n, the actual time step size will not increase the dissipation as it shrinks to zero following a similar argument as in 1D case.

Remark. If the right hand side of the equation (14) is not zero, e.g., a diffusive term, the spatial discretization for the right hand side doesn't have to be along the diagonal direction. A discretization form for the right hand side as in section 3 can be simply added to the right hand side of the scheme (18), which should be studied in the future.

6 Numerical Experiments

Example 1. We test the accuracy of the scheme (4) with various reconstruction methods and the scheme in section 4.1 for the 1D linear translation equation

$$u_t + u_x = 0, \quad x \in [0, 2],$$
$$u(x, 0) = 1 + sin(\pi x), \quad x \in [0, 2],$$

with periodic boundary condition. We set $\theta = \Delta t_n/\Delta\tau_n = 0.5$ except in the 4th order case, $\Delta\tau_n = \Delta x/2$. The final time is $T = 2$. Corresponding order (up to 3) of TVD Runge-Kutta time discretization is used for each test.

In Table 1, we show the l_1 error e_1 and l_∞ error E_1 using (4) with linear ENO reconstruction separately for two classes of cells. In Table 2, we show the l_1 error e_2 and l_∞ error E_2 using (4) with linear ENO reconstruction for combined overlapping cells. It is interesting to study the ratios e_1/e_2 and

Δx	1/10	1/20	1/40	1/80	1/160	1/320
l_1 *error* e_1	0.130	0.0499	0.0141	0.00379	0.00103	0.000273
order	-	1.38	1.82	1.90	1.88	1.92
l_∞ *error* E_1	0.147	0.0647	0.0273	0.0113	0.00459	0.00185
order	-	1.18	1.24	1.27	1.30	1.31

Table 1: Numerical errors using central scheme on overlapping cells with ENO linear reconstruction on two cell classes separately. $\theta = \Delta t_n/\Delta\tau_n = 0.5$.

E_1/E_2 listed in Table 2. In Table 3, we show the l_1 error e_3 and l_∞ error E_3 using (4) with quadratic ENO reconstruction separately for two classes of cells. In Table 4, we show the l_1 error e_4 and l_∞ error E_4 using (4) with quadratic ENO reconstruction for combined overlapping cells. The ratios e_3/e_4 and E_3/E_4 are listed in Table 4. From these 4 tables we can see that the accuracies are all within expectation. Also it seems that the error when using reconstruction for combined overlapping cells is about $1/r$ times the error when using reconstruction for two classes of cells separately, where r is the order of accuracy of the scheme. This is clearly related to the smaller distance between two overlapping cell centers. In Table 5, we show that the test scheme in section 4.1 achieves the designed accuracy.

Next we conduct a convergence test for the diagonal line method in Sec 5.1 for the following 2D translation equation

$$\begin{aligned} &u_t + (2u)_x + u_y = 0, && (x,y) \in (0,1)\times(0,1), \;\; t \in [0,1], \\ &u(x,y,0) = sin(2\pi x + 4\pi y) + \tfrac{1}{3}cos(2\pi y), && (x,y) \in (0,1)\times(0,1), \end{aligned}$$

with periodic boundary condition. The initial data is chosen to contain different frequencies and yet not to have any symmetry w.r.t. the axises or diagonal lines. Also the convection direction is chosen not parallel to any of these axises. The l_1 and l_∞ error (for the cell averages since the 1D reconstruction procedure can not fully recover a 2D function to the 3rd order accuracy) at the final time $T = 1$ are shown in Table 6. Clearly the l_1 error of the diagonal line method essentially meets the expected third order of accuracy.

Δx	1/10	1/20	1/40	1/80	1/160	1/320
l_1 *error* e_2	0.0910	0.0264	0.00728	0.00197	0.000526	0.000138
e_1/e_2	1.43	1.89	1.94	1.92	1.96	1.98
l_∞ *error* E_2	0.0908	0.0406	0.0171	0.00702	0.00285	0.00115
E_1/E_2	1.62	1.59	1.60	1.61	1.61	1.61

Table 2: Numerical errors using central scheme on overlapping cells with ENO linear reconstruction on combined cells. $\theta = \Delta t_n/\Delta\tau_n = 0.5$.

Δx	1/10	1/20	1/40	1/80	1/160	1/320
l_1 *error* e_3	0.0117	0.00147	0.000184	2.30e-05	2.88e-06	3.60e-07
order	-	2.99	3.00	3.00	3.00	3.00
l_∞ *error* E_3	0.00940	0.00118	0.000148	1.85e-05	2.32e-06	2.90e-07
order	-	2.99	3.00	3.00	3.00	3.00

Table 3: Numerical errors using central scheme on overlapping cells with ENO quadratic reconstruction on two cell classes separately. $\theta = \Delta t_n/\Delta\tau_n = 0.5$.

Δx	1/10	1/20	1/40	1/80	1/160	1/320
l_1 *error* e_4	0.00406	0.000506	6.32e-05	7.89e-06	9.86e-07	1.23e-07
e_3/e_4	2.88	2.91	2.91	2.92	2.92	2.93
l_∞ *error* E_4	0.00319	0.000400	4.99e-05	6.23e-06	7.77e-07	9.71e-08
E_3/E_4	2.95	2.95	2.97	2.97	2.99	2.99

Table 4: Numerical errors using central scheme on overlapping cells with compact ENO quadratic reconstruction on combined cells. $\theta = \Delta t_n/\Delta\tau_n = 0.5$.

Δx	1/10	1/20	1/40	1/80	1/160	1/320
l_1 *error*	0.000438	3.31e-05	3.10e-06	2.81e-07	1.76e-08	1.10e-09
order	-	3.72	3.41	3.46	4.00	4.00
l_∞ *error*	0.000342	2.59e-05	2.43e-06	2.21e-07	1.38e-08	8.63e-10
order	-	3.72	3.41	3.46	4.00	4.00

Table 5: Numerical errors using the test scheme in Sec 4.1 with $\Delta t_n = \min\{\frac{1}{2}\Delta\tau_n, \Delta x^{4/3}\}$.

Δx, Δy	1/20	1/40	1/80	1/160	1/320	1/640
l_1 *error*	0.231	0.0359	0.00464	0.000583	7.30e-05	9.22e-06
order	-	2.69	2.95	2.99	3.00	2.99
l_∞ *error*	0.379	0.0619	0.00875	0.00127	0.000203	3.66e-05
order	-	2.61	2.82	2.78	2.65	2.47

Table 6: Convergence test for the diagonal line method in Sec 5.1 with $\Delta\tau_n = 0.6\Delta x/\sqrt{5}$, $\Delta t_n = 0.48\Delta\tau_n$.

Example 2. We test the numerical dissipation for 1D Burgers equation

$$u_t + (\frac{1}{2}u^2)_x = 0, \quad x \in [0, 2]$$

with periodic boundary condition. The initial value is given as

$$u(x, 0) = 1 + sin(\pi x), \quad x \in [0, 2]$$

With $\Delta x = 0.02$, and final time $T = 0.7$. we compute the solution with scheme (4) using second order ENO reconstruction separately for two classes of cells. In Fig.7, we fix $\Delta\tau_n = \Delta x/4$ and choose $\Delta t_n = \Delta\tau_n$, $\frac{1}{2}\Delta\tau_n$ and $\frac{1}{10}\Delta\tau_n$ and $\Delta\tau_n^2$, and the corresponding results are shown clock-wisely starting from the upper left one. We find that the resolutions among them are about the same. As a comparison, in Fig.8, we compute the same problem again with the same set of Δt_n's, but with $\Delta\tau_n = \Delta t_n$. It is clear that the numerical dissipation becomes larger and larger as $\Delta\tau_n \to 0$. Only the solution in one class of the overlapping cells is shown in the graphs throughout this section unless specified.

Example 3. We test a hyperbolic-parabolic equation [15] using scheme (9) with compact quadratic ENO reconstruction for combined overlapping cells. The equation (8) is set with $f(u) = u^2$, $a(u, x, t) = 0$ if $|u| \le 0.25$; $a(u, x, t) = 0.1$ if $|u| > 0.25$. The initial value is

$$u_0(x) = \begin{cases} 1, & -\frac{1}{\sqrt{2}} - 0.4 < x < -\frac{1}{\sqrt{2}} + 0.4, \\ -1, & \frac{1}{\sqrt{2}} - 0.4 < x < \frac{1}{\sqrt{2}} + 0.4, \\ 0, & \text{otherwise.} \end{cases}$$

The final time is $T = 0.7$. We choose $\Delta\tau_n = \Delta x/2.4$ by the the CFL restriction of the hyperbolic part of the equation. The actual time step size is $\Delta t_n = \Delta x\Delta\tau_n$. We compute it with two mesh sizes $\Delta x = 1/15$; $\Delta x = 1/125$, and the results are shown in Fig. 9. Clearly the small time step size doesn't seem to degenerate the results.

Example 4. The nonlinear Buckley-Leverett problem (with a non-convex flux). The equation is $u_t + f(u)_x = 0$, with $f(u) = 4u^2/(4u^2 + (1 - u)^2)$. Initially, $u = 1$ in $[-1/2, 0]$ and $u = 0$ elsewhere in the computational domain $[-1, 1]$. We want to see if the central scheme on overlapping cells with compact quadratic ENO reconstruction on combined overlapping cells converges to the entropy solution. In Fig. 10 the computational result with

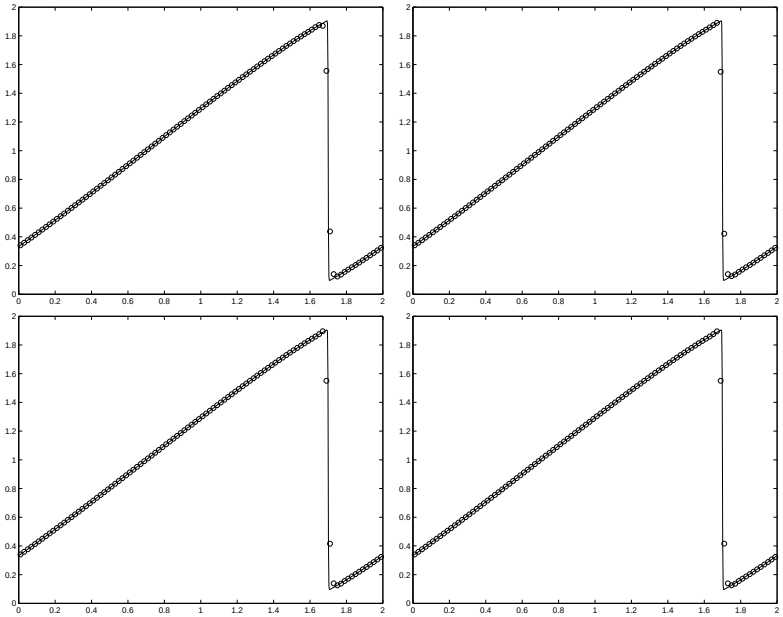

Figure 7: Comparative results for Burgers equation. $\Delta x = 0.02$, $\Delta\tau_n = \frac{1}{4}\Delta x$, $T = 0.7$. Clock-wisely from upper left: $\Delta t_n = \frac{1}{4}\Delta x$, $\frac{1}{8}\Delta x$, $\frac{1}{40}\Delta x$, $\frac{1}{16}\Delta x^2$.

$\Delta x = 1/40$ is plotted against the correct solution at $T = 0.4$. We choose $\Delta\tau_n = 0.1\Delta x$. On the left, $\Delta t_n = 0.5\Delta\tau_n$, on the right, $\Delta t_n = 0.01\Delta\tau_n$. There seems to be no major difference between them. Next we replace the ENO reconstruction with the MUSCL reconstruction on combined overlapping cells. The results are shown in Fig. 11 and they also seem to converge to the right solution. Another Riemann problem with non-convex flux (see [10]) is $f(u) = \frac{1}{4}(u^2-1)(u^2-4)$ with initial data $u(x,0) = u_l$ for $x \in [-1,0)$; $u(x,0) = u_r$ for $x \in (0,1]$; We show the results computed with central scheme on overlapping cells using compact quadratic ENO reconstruction on combined overlapping cells. On the left of Fig. 12, $u_l = 2, u_r = -2$; on the right, $u_l = -3, u_r = 3$.

Example 5. We compute the Euler equation with Lax's initial data. $u_t + f(u)_x = 0$ with $u = (\rho, \rho v, E)^T$, $f(u) = (\rho v, \rho v^2 + p, v(E+p))^T$, $p = (\gamma - 1)(E - \frac{1}{2}\rho v^2)$, $\gamma = 1.4$.

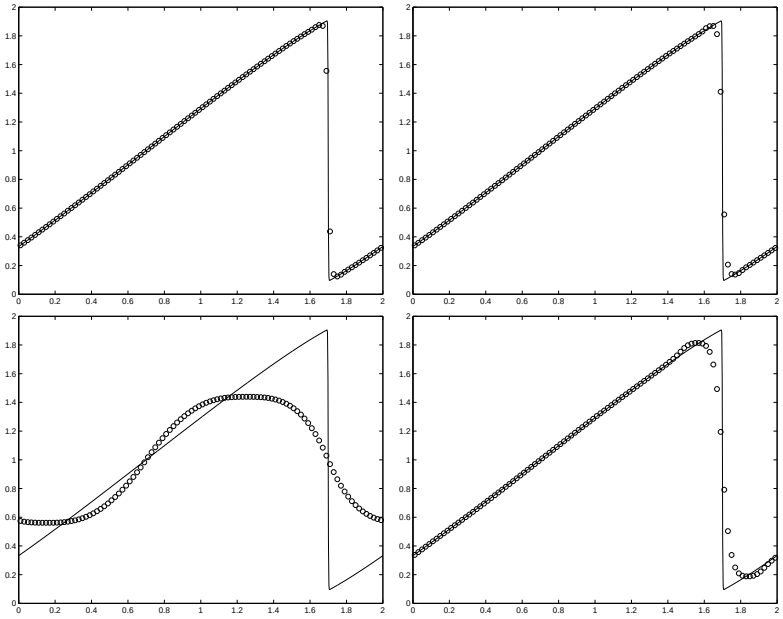

Figure 8: Comparative results for Burgers equation. $\Delta x = 0.02$, $T = 0.7$, $\Delta t_n = \Delta\tau_n$. Clock-wisely from upper left: $\Delta\tau_n = \frac{1}{4}\Delta x, \frac{1}{8}\Delta x, \frac{1}{40}\Delta x, \frac{1}{16}\Delta x^2$.

Initially, the density ρ, momentum ρv and total energy E are $0.445, 0.311, 8.928$ in $(0, 0.5)$; $0.5, 0, 1.4275$ in $(0.5, 1)$. We use central scheme (4) with quadratic ENO reconstruction. The density profile is shown at time $T = 0.16$, $\Delta x = 1/100$, $\Delta\tau_n$ is chosen with CFL factor $= 0.4$. On the left of Fig.13, reconstruction is done separately for the two classes of cells; on the right reconstruction is done for combined overlapping cells. The right ones seem to have better resolution. We also compute them with many different $\Delta t_n \in (0, \Delta\tau_n]$ and the results are very similar.

Example 6. Sod problem for Euler equation. Initially, the density, velocity, pressure are $1, 0, 1$ in $(-6, 0)$; $0.125, 0, 0.1$ in $(0, 6)$. We use central scheme on overlapping cells with compact quadratic ENO Reconstruction on combined overlapping cells, $\Delta x = 0.06$, $\Delta\tau_n$ chosen with CFL factor 0.35, $\Delta t_n = \frac{1}{2}\Delta\tau_n$ or $0.01\Delta\tau_n$. The density, velocity and pressure profiles are shown in Fig. 14 at final time $T = 2$. We can see that there is no degeneracy

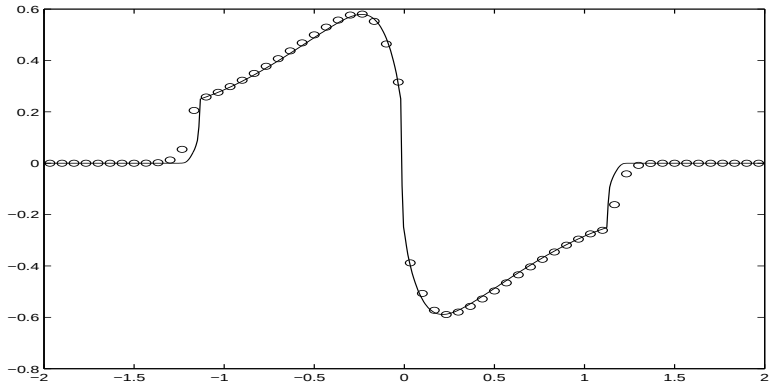

Figure 9: Hyperbolic-parabolic problem computed with central scheme on overlapping cells with compact ENO quadratic reconstruction on combined cells, $\Delta\tau_n = \Delta x/2.4$, $\Delta t_n = \Delta x \Delta\tau_n$. "o": $\Delta x = 1/15$; "-": $\Delta x = 1/125$.

by choosing very small time step size in the last graph.

Example 7. We compute the Shu-Osher problem [30] in order to test the resolution of the central schemes with different reconstructions. It is the Euler equation with initial data

$$\begin{aligned}(\rho, v, p) &= (3.857143, 2.629369, 10.333333), \quad \text{for } x < -4,\\ (\rho, v, p) &= (1 + 0.2sin(5x), 0, 1), \quad \text{for } x \geq -4.\end{aligned}$$

The density is plotted at $T = 1.8$. In Fig. 15, the density is computed using central scheme with MUSCL linear reconstruction, with $\Delta x = 1/40$, CFL factor 0.45 for $\Delta\tau_n$ and $\Delta t_n = \frac{1}{2}\Delta\tau_n$. On the left, the reconstruction is done for two classes of cells separately; on the right, the reconstruction is done for combined overlapping cells. Clearly, the right one has better resolution.

In Fig. 16, the density is computed using central scheme with ENO quadratic reconstruction, with $\Delta x = 1/20$, CFL factor 0.45 for $\Delta\tau_n$ and $\Delta t_n = \frac{1}{2}\Delta\tau_n$. On the left, the reconstruction is done for two classes of cells separately; on the right, the reconstruction is done for combined overlapping cells. The time discretization is the 3rd order TVD Runge-Kutta method. When Δt_n is getting smaller, the graphs are very similar to the ones shown. We recompute this example with the same methods with $\Delta x = 1/40$ in Fig. 17.

In Fig. 18, we put the Shu-Osher problem in $2D$ in the domain $[-5,5]\times[-0.25,0.25]$ such that initially all quantities are constant along y direction while in the x direction they are given as in the $1D$ case, $\Delta x=\Delta y=1/40$, $\Delta\tau_n$ chosen with CFL factor 0.6. The 2D Euler equation can written as

$$u_t+f(u)_x+g(u)_y=0,$$

$$u=(\rho,\rho v^x,\rho v^y,E)^T,$$

$$f(u)=(\rho v^x,\rho(v^x)^2+p,\rho v^x v^y,v^x(E+p))^T,$$

$$g(u)=(\rho v^y,\rho v^x v^y,\rho(v^y)^2+p,v^y(E+p))^T,$$

$$p=(\gamma-1)(E-\frac{1}{2}\rho((v^x)^2+(v^y)^2)),\quad \gamma=1.4.$$

We compute it with the diagonal line method with compact quadratic ENO reconstruction for combined overlapping cells. The density profile along the line $y=0$ is plotted at $T=1.8$ with two Δt_n values, $0.48\Delta\tau_n$ and $0.1\Delta\tau_n$. The results are very similar to each other which clearly shows that the dissipation is essentially independent of the actual time step size Δt_n. Also the resolution is very close to the right figure in Fig. 17, which shows that our 2D line method has almost as high resolution as its 1D version.

Example 8. Woodward and Colella problem [33] for Euler equation. Initially, the density, momentum, total energy are $1,0,2500$ in $(0,0.1)$; $1,0,0.025$ in $(0.1,0.9)$; $1,0,250$ in $(0.9,1)$. We use central scheme on overlapping cells with compact quadratic ENO reconstruction on combined overlapping cells, $\Delta x=1/400$, $\Delta\tau_n$ is chosen with CFL factor 0.45, $\Delta t_n=\frac{1}{2}\Delta\tau_n$ or $0.01\Delta\tau_n$. The density, velocity and pressure profiles are shown in Fig. 19 at final time $T=0.01$ and in Fig. 20 at times $T=0.03$ and 0.038. The density peak at graph (A) of Fig. 19 seems to be quite close to the fine solution (computed with $\Delta x=1/2000$.) Also in (D) of Fig. 19 the small time step size doesn't affect the density peak at all.

Example 9. Double Mach reflection [33]. A planar Mach 10 shock is incident on an oblique wedge at a $\pi/3$ angle. The air in front of the shock has density 1.4, pressure 1 and velocity 0. The boundary condition is described in [33]. We compute the problem with central scheme on overlapping cells using diagonal line method with compact quadratic ENO reconstruction on combined overlapping cells. The density and pressure profiles are plotted at final time $T=0.2$ in Fig. 21 with 50 equally spaced contours. The first two

graphs are computed with $\Delta x = 1/60$, and the third graph is computed with $\Delta x = 1/120$.

Example 10. 2D Riemann problems. We compute two 2D Riemann problems (see [19]) for Euler equation with central scheme on overlapping cells using diagonal line method with compact quadratic ENO reconstruction on combined overlapping cells.

The computational domain is $[0,1]\times[0,1]$. The initial states are constants within each of the 4 quadrants. Counter-clock-wisely from the upper right quadrant, they are labeled as $(\rho_i, v_i^x, v_i^y, p_i)$, $i = 1,2,3,4$. In Fig. 22, the initial data are $\rho_1 = 1.1$, $v_1^x = 0$, $v_1^y = 0$, $p_1 = 1.1$, $\rho_2 = 0.5065$, $v_2^x = 0.8939$, $v_2^y = 0$, $p_2 = 0.35$, $\rho_3 = 1.1$, $v_3^x = 0.8939$, $v_3^y = 0.8939$, $p_3 = 1.1$, $\rho_4 = 0.5065$, $v_4^x = 0$, $v_4^y = 0.8939$, $p_4 = 0.35$. We compute it with $\Delta x = 1/200$, $\Delta\tau_n$ chosen with CFL factor 0.6 and $\Delta t_n = 0.4\Delta\tau_n$. The density and pressure contours are shown at final time $T = 0.25$.

In Fig. 23, the initial data are $\rho_1 = 1.5$, $v_1^x = 0$, $v_1^y = 0$, $p_1 = 1.5$, $\rho_2 = 0.5323$, $v_2^x = 1.206$, $v_2^y = 0$, $p_2 = 0.3$, $\rho_3 = 0.138$, $v_3^x = 1.206$, $v_3^y = 1.206$, $p_3 = 0.029$, $\rho_4 = 0.5323$, $v_4^x = 1.206$, $v_4^y = 1.206$, $p_4 = 0.3$. We compute it with $\Delta x = 1/400$, $\Delta\tau_n$ chosen with CFL factor 0.6 and $\Delta t_n = 0.4\Delta\tau_n$. The density and pressure contours are shown at final time $T = 0.3$.

7 Concluding Remarks.

We have developed central schemes on overlapping cells which simplify the time discretization. By use of a convex combination of the two classes of overlapping cell averages, the $O(1/\Delta t)$ dependent dissipation error can be removed. We also show that combining the two classes of overlapping cells in reconstruction, if properly done, will not cause any problem. In fact, it improves the accuracy and resolution of the scheme. The techniques we have developed could be easily applied to unstructured staggered grids. All these benifits should be able to compensate for the extra computational cost associated with the use of overlapping cells.

References

[1] P. Arminjon and A. St-Cyr, Nessyahu-Tadmor-type central finite volume methods without predictor for 3D Cartesian and unstructured tetrahedral

grids, *Appl. Numer. Math.* **46** (2003), no. 2, 135–155.

[2] P. Arminjon and M.-C. Viallon, Convergence of a finite volume extension of the Nessyahu-Tadmor scheme on unstructured grids for a two-dimensional linear hyperbolic equation, *SIAM J. Numer. Anal.* **36** (1999), 738–771.

[3] R. Abgrall, On essentially non-oscillatory schemes on unstructured meshes: analysis and implementation, *J. Comput. Phys.* **114** (1994), 45-58.

[4] T. Barth and P. Frederickson, High order solution of the Euler equations on unstructured grids using quadratic reconstruction, *AIAA* Paper No. 90-0013.

[5] F. Bianco, G. Puppo and G. Russo, High-order central schemes for hyperbolic systems of conservation laws, *SIAM J. Sci. Comput.* **21** (1999), no. 1, 294–322.

[6] S. Bryson and D. Levy, High-order central WENO schemes for multidimensional Hamilton-Jacobi equations, *SIAM J. Numer. Anal.*, **41** (2003), 1339–1369.

[7] J. Glimm, X.-L. Li and A.-D. Lin, Nonuniform approach to terminal velocity for single mode Rayleigh-Taylor instability, *Acta Math. Appl. Sin. Engl. Ser.* **18** (2002), no. 1, 1–8.

[8] J. Glimm, X.-L. Li, Y. Liu, Z. Xu and N. Zhao, Conservative Front Tracking with Improved Accuracy, *SIAM J. Numer. Anal.*, **41** (2003), 1926-1947.

[9] A. Harten, High resolution schemes for hyperbolic conservation laws, *J. Comput. Phys.* **49** (1983), no. 3, 357–393.

[10] A. Harten, B. Engquist, S. Osher and S. R. Chakravarthy, Uniformly high-order accurate essentially non-oscillatory schemes, III, *J. Comput. Phys.* **71** (1987), no. 2, 231–303.

[11] G.-S. Jiang, D. Levy, C.-T. Lin, S. Osher and E. Tadmor, High-resolution non-oscillatory central schemes with non-staggered grids for hyperbolic conservation laws, *SIAM J. Numer. Anal.* **35** (1998), 2147.

[12] G.-S. Jiang and E. Tadmor, Non-oscillatory central schemes for multidimensional hyperbolic conservation laws, *SIAM J. Sci. Comput.* **19** (1998), no. 6, 1892–1917.

[13] S. Jin and Z. Xin, The relaxation schemes for systems of conservation laws in arbitrary space dimensions, *Comm. Pure Appl. Math.* **48** (1995), no. 3, 235–276.

[14] A. Kurganov and D. Levy, A third-order semi-discrete central scheme for conservation laws and convection-diffusion equations, *SIAM J. Sci. Comput.* **22** (2000), no. 4, 1461–1488.

[15] A. Kurganov and E. Tadmor, New high-resolution central schemes for nonlinear conservation laws and convection-diffusion equations, *J. Comput. Phys.* **160** (2000), no. 1, 241–282.

[16] A. Kurganov and E. Tadmor, New high-resolution semi-discrete central schemes for Hamilton-Jacobi equations, *J. Comput. Phys.* **160** (2000), 720–742.

[17] A. Kurganov and G. Petrova, A third-order semi-discrete genuinely multidimensional central scheme for hyperbolic conservation laws and related problems. *Numer. Math.*, **88** (2001), no. 4, 683–729.

[18] P.D. Lax, Weak solutions of nonlinear hyperbolic equations and their numerical computation, *Comm. Pure Appl. Math.* **7** (1954), 159–193.

[19] P. Lax and X.-D. Liu, Solution of Two Dimensional Riemann Problem of Gas Dynamics by Positive Schemes, *SIAM J. Sci. Comput.* **19** (1998), No 2, pp.319-340.

[20] D. Levy, G. Puppo and G. Russo, Central WENO schemes for nonlinear conservation laws, *Math. Model. Numer. Anal.*, **33** (1999), 547.

[21] D. Levy, G. Puppo and G. Russo, Compact central WENO schemes for multidimensional conservation laws, *SIAM J. Sci. Comput.* **22** (2000), no. 2, 656–672.

[22] D. Levy, G. Puppo and G. Russo, A fourth-order central WENO scheme for multidimensional hyperbolic systems of conservation laws, *SIAM J. Sci. Comput.* **24** (2002), no. 2, 480–506.

[23] X.-D. Liu and S. Osher, Convex ENO high order multi-dimensional schemes without field by field decomposition or staggered grids, *J. Comput. Phys.* **142** (1998), no. 2, 304–330.

[24] X.-D. Liu, S. Osher and T. Chan, Weighted essentially non-oscillatory schemes, *J. Comput. Phys.* **115** (1994), no. 1, 200–212.

[25] X.-D. Liu and E. Tadmor, Third order nonoscillatory central scheme for hyperbolic conservation laws, *Numer. Math.* **79** (1998), no. 3, 397–425.

[26] H. Nessyahu and E. Tadmor, Nonoscillatory central differencing for hyperbolic conservation laws, *J. Comput. Phys.* **87** (1990), no. 2, 408–463.

[27] J. Qiu and C.-W. Shu, On the construction, comparison, and local characteristic decomposition for high-order central WENO schemes, *J. Comput. Phys.* **183** (2002), no. 1, 187–209.

[28] C.-W. Shu, Essentially non-oscillatory and weighted essentially non-oscillatory schemes for hyperbolic conservation laws, in Advanced Numerical Approximation of Nonlinear Hyperbolic Equations, A. Quarteroni, ed., *Lecture Notes in Math.* **1697** (1998), Springer, Berlin.

[29] C.-W. Shu and S. Osher, Efficient implementation of essentially non-oscillatory shock-capturing schemes, *J. Comput. Phys.* **77** (1988), no. 2, 439–471.

[30] C.-W. Shu and S. Osher, Efficient implementation of essentially nonoscillatory shock-capturing schemes, II, *J. Comput. Phys.* **83** (1989), no. 1, 32–78.

[31] H.-Z. Tang and T. Tang, Adaptive mesh methods for one- and two-dimensional hyperbolic conservation laws *SIAM J. Numer. Anal.* **41** (2003), 487–515.

[32] B. van Leer, Towards the ultimate conservative difference scheme V, A second-order sequel to Godunov's method, *J. Comput. Phys.* **32** (1979), 101–136.

[33] P. Woodward and P. Colella, The numerical simulation of two-dimensional fluid flow with strong shocks, *J. Comput. Phys.* **54** (1984), no. 1, 115–173.

[34] M. Zennaro, Natural continuous extensions of Runge-Kutta methods, *Math. Comput.* **46** (1986), 119.

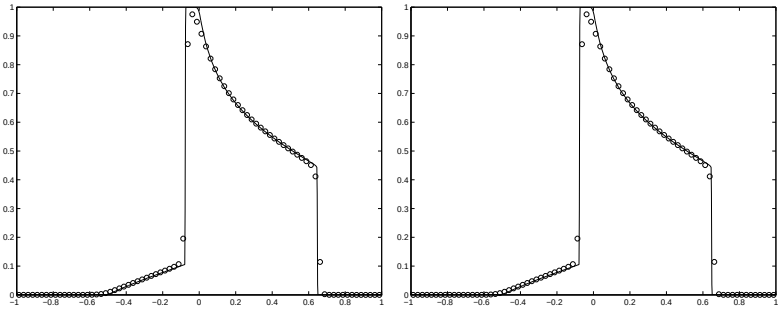

Figure 10: Buckley-Leverett Problem computed with central scheme on overlapping cells with compact quadratic ENO reconstruction on combined overlapping cells. $\Delta x = 1/40$, $T = 0.4$, $\Delta\tau_n = 0.1\Delta x$. Left: $\Delta t_n = 0.5\Delta\tau_n$. Right: $\Delta t_n = 0.01\Delta\tau_n$.

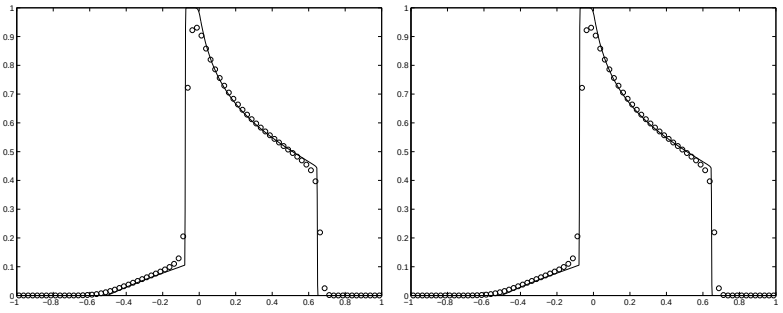

Figure 11: Buckley-Leverett Problem computed with central scheme on overlapping cells with MUSCL reconstruction on combined overlapping cells. $\Delta x = 1/40$, $T = 0.4$, $\Delta\tau_n = 0.1\Delta x$. Left: $\Delta t_n = 0.5\Delta\tau_n$. Right: $\Delta t_n = 0.01\Delta\tau_n$.

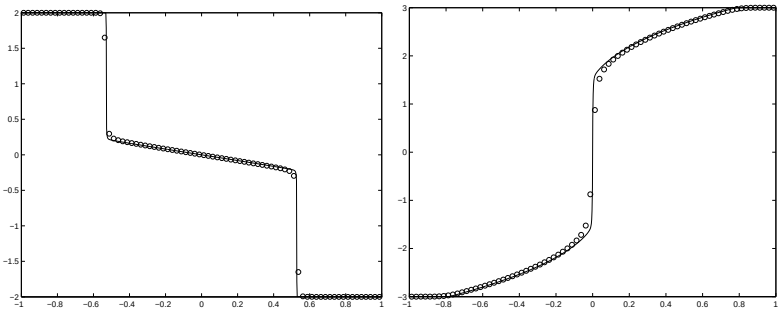

Figure 12: Riemann problems with non-convex flux, $\Delta x = 1/40$. Left: $u_l = 2, u_r = -2$, $\Delta\tau_n = 0.15\Delta x$, $\Delta t_n = \frac{1}{2}\Delta\tau_n$. Right: $u_l = -3, u_r = 3$, $\Delta\tau_n = 0.02\Delta x$, $\Delta t_n = \frac{1}{2}\Delta\tau_n$.

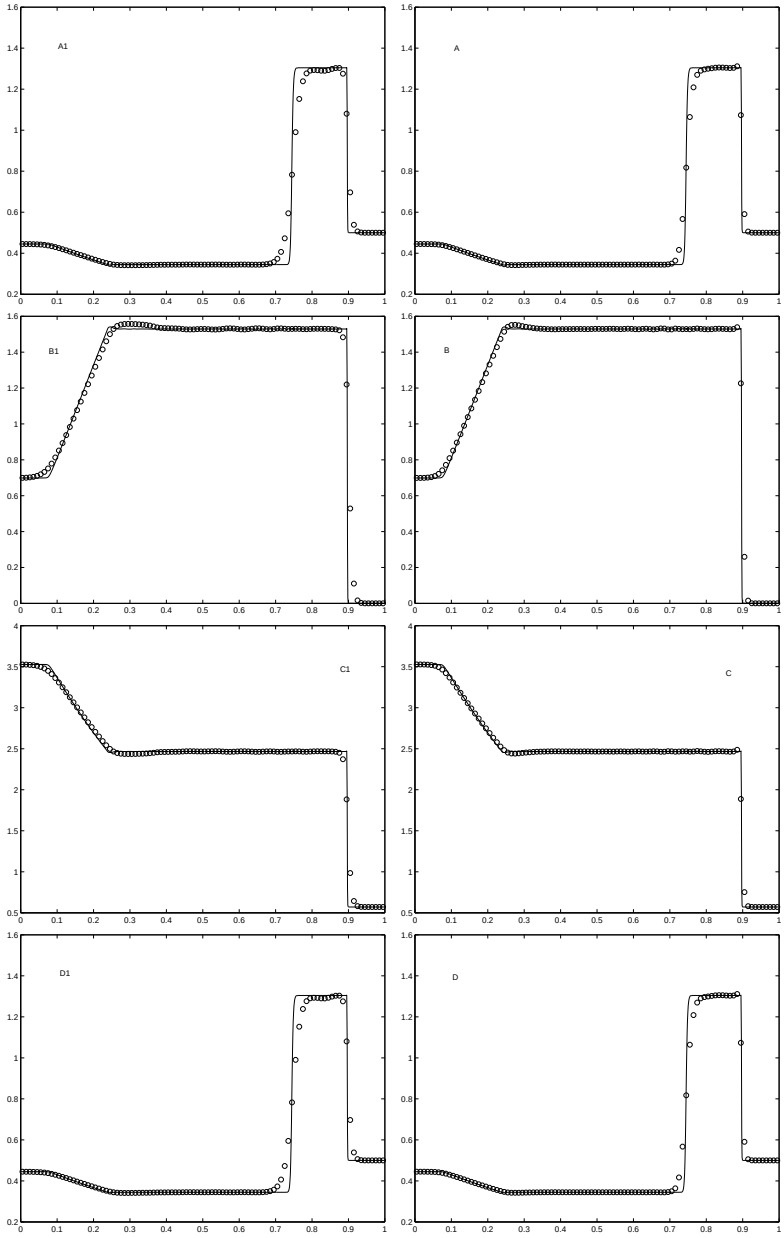

Figure 13: Comparative results for Lax's Problem computed by Central scheme on overlapping cells, $\Delta x = 1/100$, $\Delta\tau_n$ chosen with CFL factor 0.4, $\Delta t_n = 0.5\Delta\tau_n$ by default. Left: ENO quadratic reconstruction separately for two classes of cells, (A1)density; (B1)velocity; (C1)pressure; (D1)density, $\Delta t_n = 0.01\Delta\tau_n$. Right: compact ENO quadratic reconstruction for combined overlapping cells, (A)density; (B)velocity; (C)pressure; (D)density, $\Delta t_n = 0.01\Delta\tau_n$.

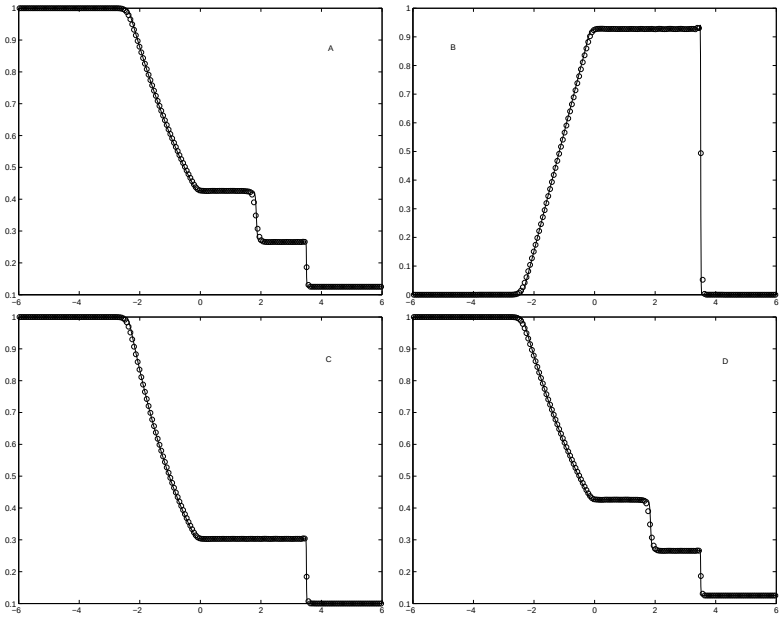

Figure 14: Sod Problem, $\Delta x = 0.06$, $T = 2$, $\Delta\tau_n$ chosen with CFL factor 0.35, $\Delta t_n = \frac{1}{2}\Delta\tau_n$ by default. (A)Density; (B)Velocity; (C)Pressure; (D)Density, $\Delta t_n = 0.01\Delta\tau_n$.

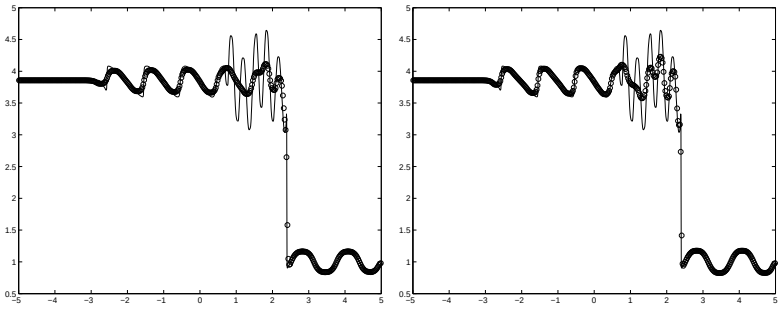

Figure 15: Shu-Osher Problem computed with Central schemes on overlapping cells using MUSCL reconstruction with minmod limiter, $\Delta x = 1/40$, $\Delta t_n = \frac{1}{2}\Delta\tau_n$, $\Delta\tau_n$ chosen with CFL factor 0.45. Left: reconstruction done separately for two cell classes. Right: reconstruction done for combined overlapping cells.

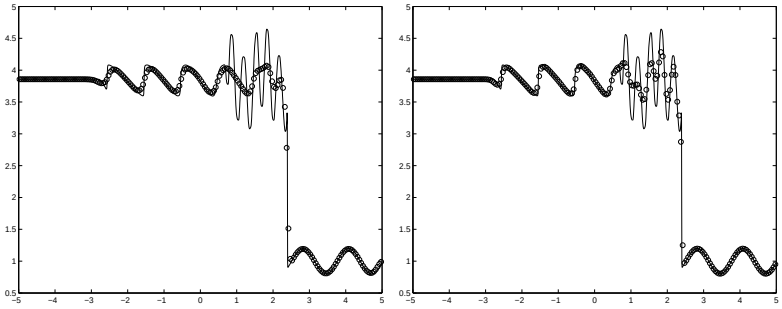

Figure 16: Shu-Osher Problem computed with Central schemes on overlapping cells using quadratic ENO reconstruction, $\Delta x = 1/20$, $\Delta t_n = \frac{1}{2}\Delta\tau_n$, $\Delta\tau_n$ chosen with CFL factor 0.45. Left: reconstruction done separately for two cell classes. Right: reconstruction done for combined overlapping cells.

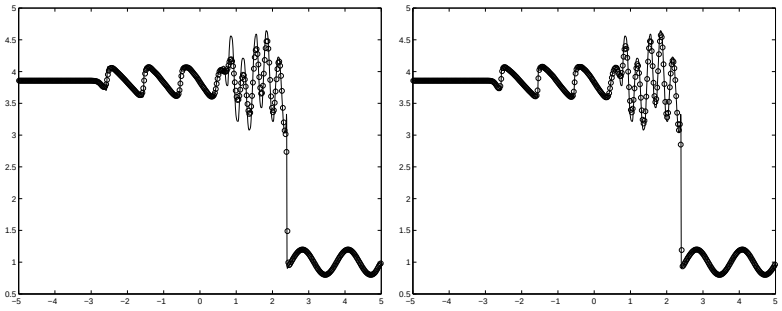

Figure 17: Shu-Osher Problem computed with Central schemes on overlapping cell, $\Delta x = 1/40$, $\Delta t_n = \frac{1}{2}\Delta\tau_n$, $\Delta\tau_n$ chosen with CFL factor 0.45. Left: reconstruction done separately for two cell classes. Right: reconstruction done for combined overlapping cells.

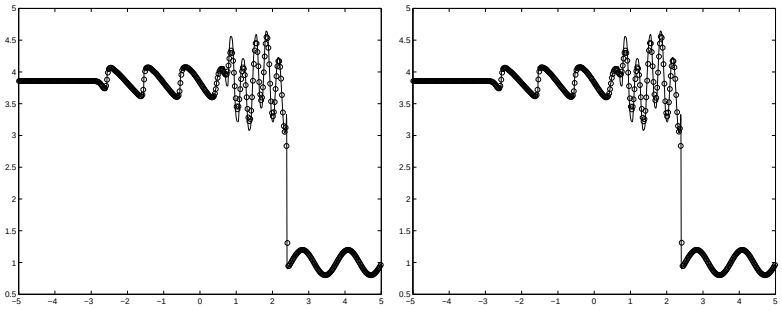

Figure 18: 2D Shu-Osher Problem computed with central scheme on overlapping cells using diagonal line method with compact quadratic ENO reconstruction on combined overlapping cells, $\Delta x = \Delta y = 1/40$, $\Delta\tau_n$ chosen with CFL factor 0.6. The density profiles along $y = 0$ are shown. Left: $\Delta t_n = 0.48\Delta\tau_n$; Right: $\Delta t_n = 0.1\Delta\tau_n$.

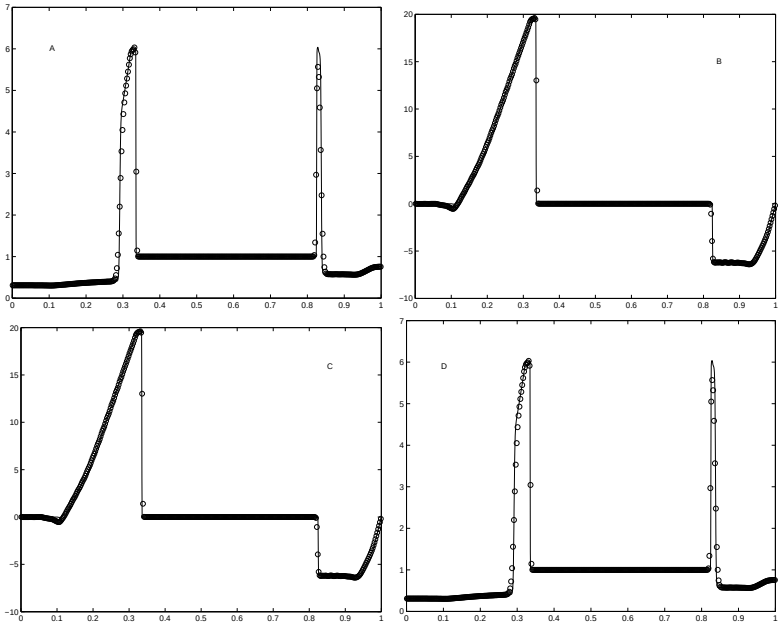

Figure 19: Woodward and Colella Problem computed with central scheme on overlapping cells with compact quadratic ENO reconstruction for combined overlapping cells, $\Delta x = 1/400$, $T = 0.01$, $\Delta\tau_n$ chosen with CFL factor 0.45, $\Delta t_n = \frac{1}{2}\Delta\tau_n$ by default. (A) density; (B)velocity; (C)pressure; (D)density, $\Delta t_n = 0.01\Delta\tau_n$.

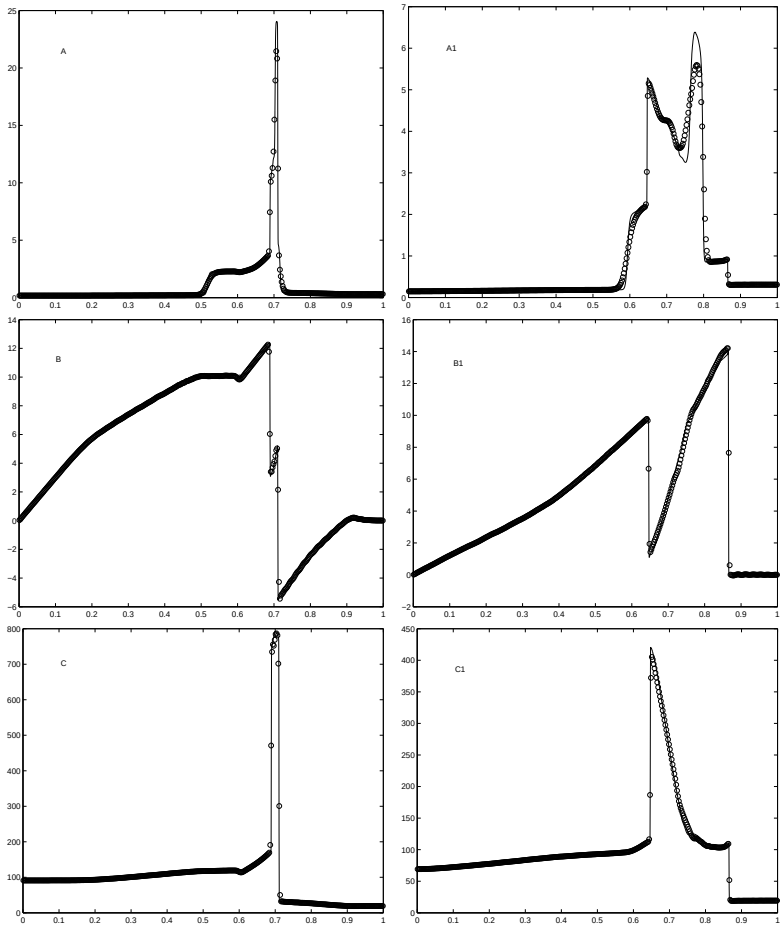

Figure 20: Woodward and Colella Problem computed with central scheme on overlapping cells with compact quadratic ENO reconstruction for combined overlapping cells, $\Delta x = 1/400$, $\Delta\tau_n$ chosen with CFL factor 0.45 , $\Delta t_n = \frac{1}{2}\Delta\tau_n$. On the left, $T = 0.03$, (A) density; (B)velocity; (C)pressure. On the right, $T = 0.038$, (A1) density; (B1)velocity; (C1)pressure.

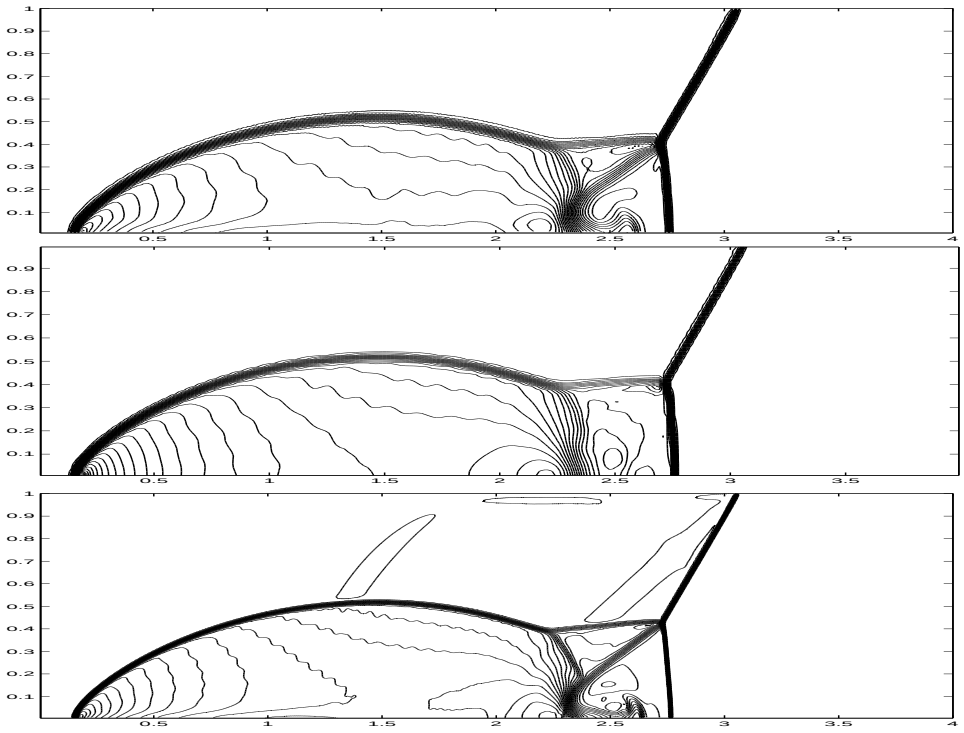

Figure 21: Double Mach reflection computed with central scheme on overlapping cells using diagonal line method with compact quadratic ENO reconstruction on combined overlapping cells, $\Delta y = \Delta x$, $\Delta\tau_n$ chosen with CFL factor 0.6, $\Delta t_n = 0.4\Delta\tau_n$. Upper: density, $\Delta x = 1/60$; Middle: pressure, $\Delta x = 1/60$; Lower: density, $\Delta x = 1/120$.

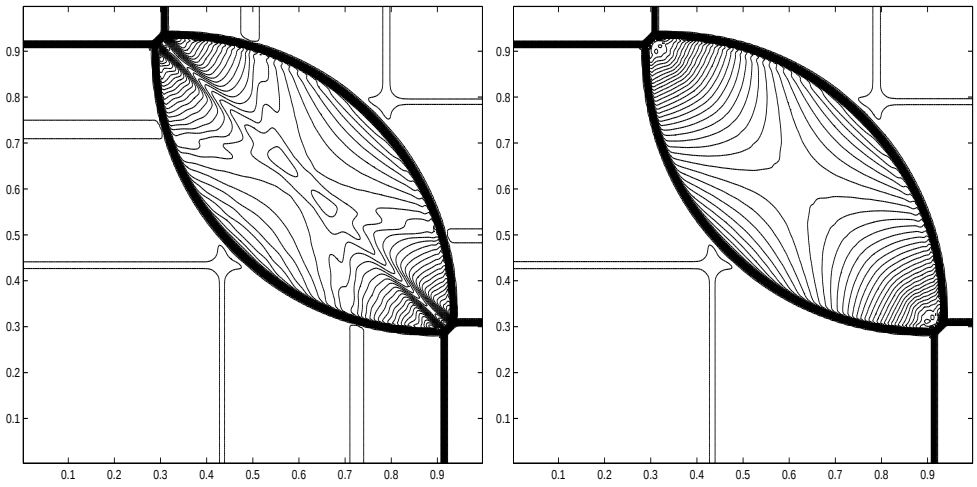

Figure 22: 2D Riemann problem 1. $\Delta x = \Delta y = 1/200$, $\Delta\tau_n$ chosen with CFL factor 0.6, $\Delta t_n = 0.4\Delta\tau_n$. Left: density; Right: pressure

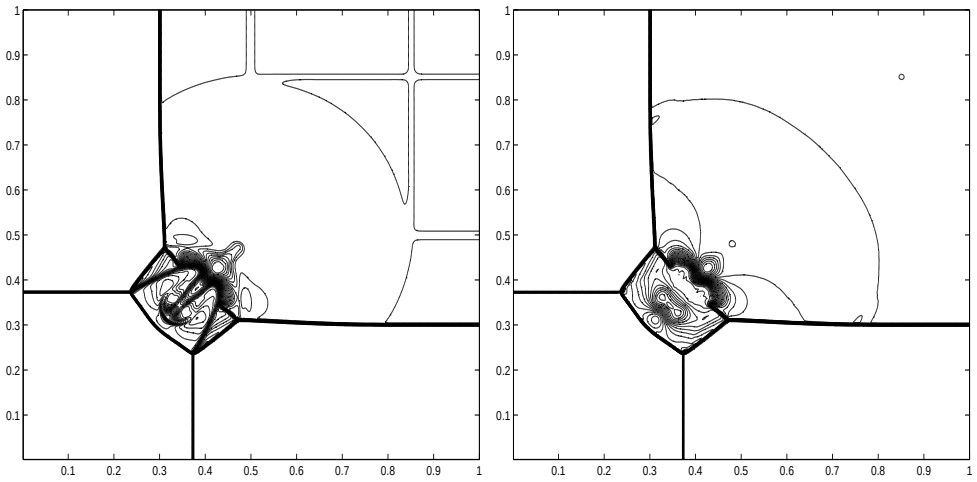

Figure 23: 2D Riemann problem 2. $\Delta x = \Delta y = 1/400$, $\Delta\tau_n$ chosen with CFL factor 0.6, $\Delta t_n = 0.4\Delta\tau_n$. Left: density; Right: pressure